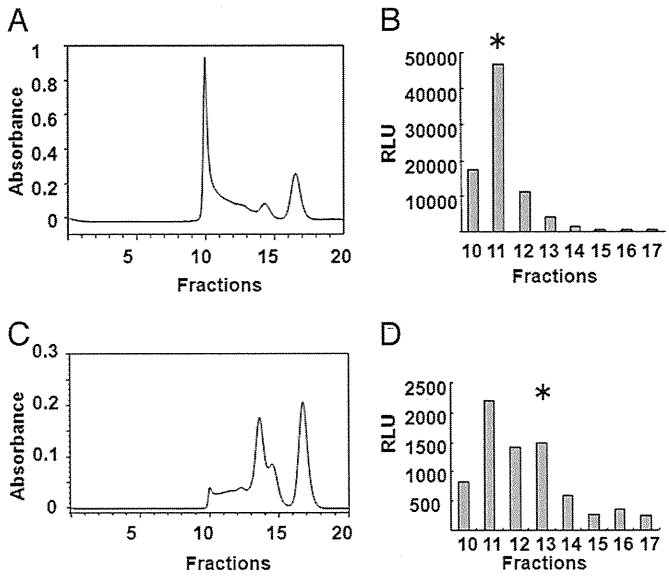

Fig. 3. Antibodies linked to avidin. (*A*) Purification of avidin-bound antibody by gel filtration column chromatography on TSK gel G3000SW column. (*B*) Bioluminescence ELISA was used to detect antibody-avidin conjugates; asterisk represents collected fraction. (*C*) Purification of reduced antibody-avidin by gel filtration column chromatography. (*D*) Bioluminescent ELISA was used to detect reduced antibody-avidin conjugates; asterisk represents collected fraction. RLU, relative luminescence unit.

We developed several tumor-bearing nude mice xenografted with Dlk-1-positive Huh-7 cells (Fig. 5*A* and *B* and Fig. S2*A* and *B*). At 24 h postinjection of CLuc-IgG (upper panels) or FBP-IgG (lower panels), the mice were injected with a solution of *Cypridina* luciferin, and 5–10 min later, BLI were obtained using a commercial CCD imaging system. The images (Fig. 5 *C* and *D*) showed that both Cluc-IgG and FBP-IgG probes were visible at the tumor site, with that from FBP-IgG two fold higher than that of CLuc-IgG, and the signal to noise ratio also improved. To determine if BRET occurs in these live animals, we measured

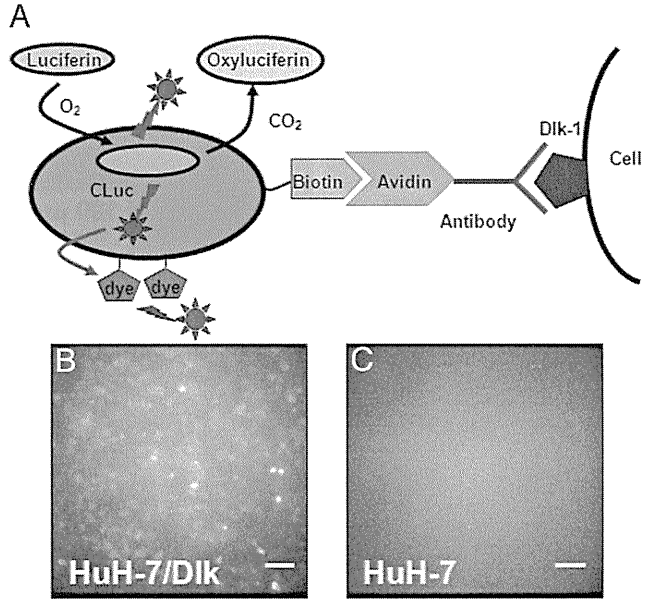

Fig. 4. (*A*) Schematic of FBP-IgG showing targeting to tumor cells. (*B*) BLI of Dlk-1-positive Huh-7/Dlk cells. (*C*) BLI of Dlk-1-negative Huh-7 cells. (Scale bars, 200 μm).

BLI in the presence of the 570 nm long pass filter. The signal from FBP at the tumor site (Fig. 5*F*) was significantly higher than that of CLuc (Fig. 5*E*), showing that the BRET system was active.

Fluorescence imaging of the mice was performed just before luciferin injection using the same CCD imaging system and a set of Cy-5 filters. Although CLuc-IgG does not contain the fluorescent dye, autofluorescence from tissue was observed (Fig. 5*G*). During the initial 20 min after the injection of FBP-IgG, we observed a strong fluorescent signal from the whole of the animal, because of blood circulation (Fig. 5*H*). However, at 24 h postinjection of the imaging probes, fluorescence images showed little difference between CLuc and FBP of fluorescent signals at tumor sites (Fig. 5 *I* and *J*). In addition, at 48 h postinjection, bioluminescence images and fluorescence images were similar to those seen at 24 h postinjection (Fig. S2 *C*–*J*).

Discussion

The use of luciferase as a bioluminescent tag is a convenient and clean approach for in vivo imaging with advantages over radioactivity; also, background is much lower with bioluminescence than with fluorescence. CLuc is a well-known bioluminescent enzyme. Its high quantum yield and turnover-rate makes it a sensitive reporter in small animals as well as in vitro. A limiting factor for the use of CLuc as a bioluminescent tag for in vivo imaging is the blue emission that overlaps with the absorption spectrum of hemoglobin. In the present study, we chose an organic dye as the energy acceptor for BRET with CLuc because of its low molecular weight. The bioluminescence spectrum of CLuc overlaps a part of the absorption spectrum of the dye (Fig. S3). BRET efficiency was estimated to be 0.3, based on the ratio of light intensity at 675 nm to that at 460 nm (Fig. 1*C*). A possible alternative approach would be the use of a luciferase system that emits red light, such as the railroad worm *Phrixothrix*, whose emission peaks at 628 nm, Although we have not evaluated this system, its recombinant luciferase may not be suitable as it is an unstable protein (27). Furthermore its bioluminescent system requires the cofactor ATP, which is not available in extra-cellular environments.

For the detection of liver cancer cells, we prepared a monoclonal antibody against Huh-7 cells expressing Dlk-1. Chemical conjugation of the anti-Dlk-1 antibody to avidin yielded a high molecular weight complex (Fig. 3*A*). We obtained high-resolution microscopic BLI using the avidin-bound unreduced antibody and FBP (Fig. 4*B*), an example of such imaging in single isolated antigen-expressing cells without an external light source. On the other hand, we found that its utility in live animals was poor (Fig. S4). Therefore, we conjugated the reduced antibody to avidin for in vivo imaging, and found that it can be used to target the cell surface antigen despite its low avidity compared to full antibody. Previous studies have shown that fusion of antibody fragments with a luciferase is another efficient way to label antigens on the cell surface (28, 29). However, our chemical conjugation is more easily applicable to the preparation of other CLuc-antibody probes targeting various disease-specific markers, because many antibodies are commercially available.

We found that FBP displayed a 2-fold increase in light output versus CLuc as a bioluminescent tag for in vivo imaging (Fig. 5 *C* and *D*). Since CLuc and FBP use the same luciferase and luciferin, the increased light emission in the far-red part of the spectrum is the direct cause of the improvement of the signal to noise ratio. With fluorescence imaging, we found several difficulties for tumor-specific detection. The images (Fig. 5*G*) show fluorescence signals from the CLuc-IgG mouse because of endogenous fluorophores. In the mouse injected with excess amount of FBP (20 μg), we found a strong fluorescence signal from the whole body (Fig. 5*H*). However, little difference

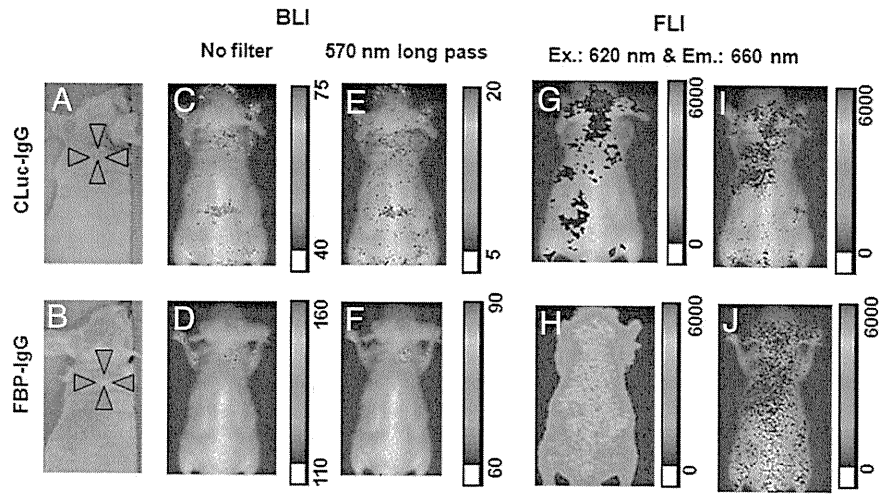

Fig. 5. Images of live animals. (*A* and *B*) Photographs of two tumor-bearing mice. (*C* and *D*) 24 h after the administration of CLuc-IgG or FBP-IgG, luciferin was injected and the bioluminescence images (BLIs) were obtained using a CCD photon imaging system. Color scale, photons/s/steradian. (*E* and *F*) The bioluminescence images were obtained with 570 nm long-pass filter. (*G* and *H*) Fluorescence images (FLIs) of tumor-bearing mice shown in panels *A* and *B* immediately after the administration of CLuc-IgG or FBP-IgG were obtained with the same CCD photon imaging system and a set of Cy5 filters. (*I* and *J*) FLIs of the tumor-bearing mice shown in panels *A* and *B* 24 h after administration of CLuc-IgG or FBP-IgG, but before luciferin injection, were obtained under same conditions.

between tumor sites and normal tissues were observed at 24 h (Fig. 5*J*) and 48 h (Fig. S2*J*).

In summary, we have established a bioluminescent protein based on CLuc and a fluorescent dye. This BRET system can be used in the imaging of tumor tissues in small animals. Meanwhile the performance of FBP has been shown to be better than that of CLuc in vivo. Although little is known about the toxicity of *Cypridina* luciferin and *Cypridina* luciferase, and this remains to be investigated, this FBP offers a very useful analytical tool for the evaluations of monoclonal antibody localization in live animals.

Materials and Methods

Preparation of FBP. A mixture of 0.1 mg biotinylated CLuc and 1 μmol sodium metaperiodate in 0.1 ml of 0.1 M sodium acetate buffer (pH 5.2) was incubated at 4 °C for 30 min. To stop the reaction, glycerol was added to a final concentration of 15 mM. The reaction mixture was incubated at 4 °C for 5 min and then loaded onto a size-exclusion column. Oxidized biotinylated CLuc was eluted with 0.1 M sodium acetate buffer (pH 5.2). Fractions giving strong bioluminescence signals were pooled and concentrated using an Ultrafree-0.5 centrifugal filter device and an equivalent volume of 10 mM HiLyte Fluor™ 647 hydrazide (AnaSpec) in 0.1 M sodium acetate buffer (pH 5.2) was added. The mixture was incubated at room temperature for 2 h, and then loaded onto a size-exclusion column, and FBP was eluted with the 0.1 M potassium phosphate buffer (pH 7.2) containing 0.15 M NaCl. Fractions showing strong bioluminescence signals were combined and stored at 4 °C until use. Bioluminescence emission spectra were measured by mixing 0.1 mM *Cypridina* luciferin and FBP in various buffers on an ATTO AB-1850 LumiFL-Spectrocapture. To determine the effects of pH on the bioluminescence spectra, a 100 mM sodium phosphate buffer (pH 6.5), 100 mM Tris-HCl buffer (pH 7.4) or 100 mM Tris-HCl buffer (pH 8) containing 0.1 M NaCl were used. To determine the effects of high ion concentration on bioluminescence spectra, the same buffers containing 0.5 M NaCl was used, while to determine the effect of hemoglobin on the bioluminescence spectra, 100 mM Tris-HCl buffer containing 0.1 M NaCl and 150 mg/mL hemoglobin was used. All spectra were normalized. Relative light intensity was measured by the addition of Cypridina luciferin (40 ng) to the PBS buffer (100 μL) or blood (100 μL) containing either FBP (25 ng) or CLuc (25 ng).

Isolation of Full-Length Dlk-1 cDNA from Human. PCR primers were designed based on the gene sequences of human Dlk-1 (GenBank accession no. U15979). Sequences of the prepared primers were as follows: forward primer: 5′-cgc-gtc-cgc-aac-cag-aag-ccc-3′ and reverse primer: 5′-aag-ctt-gat-ctc-ctc-gtc-gcc-ggc-c-3′. To the reverse primer, *Hin*dIII restriction site was added. PCR was performed using these primers and cDNAs synthesized from total RNAs prepared from human liver at embryonic week 10 (TaKaRa). PCR product was cloned into PCRII vector (Invitrogen) (pCRII-hdlk-1). To construct the expression vector, Flag tag sequences were inserted into the *Hin*dIII/*Sal*I site of pBluescript II SK(+) vector (Stratagene) (pBS-Flag). Then, an *Eco*RI/*Hin*dIII fragment was cleaved off from pCRII-hdlk-1 and inserted into the *Eco*RI/*Hin*dIII site of pBS-Flag vector (pBS-hdlk-1-Flag). An *Eco*RI/*Sal*I fragment was cleaved off from pBS-hdlk-1-Flag and inserted into the *Eco*RI/*Xho*I site of pcDNA3.1 vector (Invitrogen) (pcDNA-hdlk-1-Flag).

Generation of Cell Lines Stably Expressing Dlk-1. The HEK293 cell and Huh-7 cell line derived from human liver cancer were furnished by the Japan Health Sciences Foundation. The expression vector pcDNA-hdlk-1-Flag was introduced into those cell lines using LipofectAMINE-plus reagent (Invitrogen), in accordance with the manufacturer's instruction. After selection with G418 antibiotic (Geneticin, Calbiochem), the HEK293-hdlk-1 and the Huh-7-hdlk-1 cell line that stably expresses human Dlk-1 were established.

Generation of Anti-Dlk-1 Monoclonal Antibody. Mice (BALB/c) were immunized with HEK293 cells that stably express human Dlk-1 or with the expression vector that encodes full-length human Dlk-1 cDNA. Hybridomas were generated by fusion of B cells to mouse myeloma cells (P3-X63-Ag8.653 or SP2/0-Ag14) by a conventional method. After selection with HAT supplement (Invitrogen) containing media, hybridoma clones each of which produces an anti-human Dlk-1 monoclonal antibody were screened by ELISA and flow cytometry. To prepare purified antibody protein, the hybridoma clone was i.p. administered to BALB/c nude mice at a dose of 3×10^6 cells, which was treated with 2,6,10,14-tetramethylpentadecane (pristane) 7 days before administration. After collection of ascites, the monoclonal antibody (DI-2–20) was purified with a protein G column (GE Healthcare).

Immunostaining and Western Blot Analyses. For immunocytostaining, Huh-7/Dlk and Huh-7 cells were cultured and fixed with ice-cold 100% methanol. Hoechst33342 was used for nuclear staining. Newly developed anti-human Dlk-1 monoclonal antibody (DI-2–20) and a goat FITC-labeled anti-mouse IgG (Santa Cruz Biotechnology) were used for Dlk-staining. For western blot analysis, Huh-7/Dlk and Huh-7 cells were harvested and whole cell protein extracts were prepared. Thirty μg protein was separated by 10% SDS/PAGE and transferred to a nitrocellulose membrane. An anti-human Dlk-1 monoclonal antibody (DI-2–20) and goat anti-mouse IgG (Santa Cruz Biotechnology) were used as primary and secondary antibodies, respectively.

Avidin Antibody. Conjugation of anti-human Dlk-1 monoclonal antibody or reduced antibody to avidin was performed with EZ-link maleimide activated NeutrAvidin™ protein, in accordance with the manufacturer's instruction (Pierce). The avidin-bound antibody was purified by gel filtration column chromatography using a TSK gel G3000SW column (Tosoh). Collected fractions were diluted and then added to a 96-well plate precoated with goat anti-mouse IgG. After the plate was washed, a solution of FPB was added and

incubation was carried out. Bioluminescent measurements were performed with a 96-well plate reader (Berthold Technologies) after adding of 100 μL of 1 μM Cypridina luciferin solution (0.1 M Tris-HCl pH7.4/0.3 M sodium ascorbate/0.02 M sodium sulfite) to each well.

Living-Cell BLI. For live-cell BLI, Huh-7/Dlk and Huh-7 cells were cultured and washed with cold PBS buffer containing 1% BSA (1% BSA/PBS). Each cell line was incubated with the probe solution containing avidin-bound antibody (25 μg) and FBP (25 μg), diluted with 1% BSA/PBS buffer at 4 °C for 120 min, and then washed three times with 1% BSA/PBS buffer. PBS buffer containing *Cypridina* luciferin (1 μM) was added to detect luminescence from the probes on the cell surface. Light was measured with Cellgraph™ (ATTO Co.) with 5-min exposure.

Optical Imaging in Live Animals. Six-week-old male BALB/c nu/nu mice each weighing ≈20 g were obtained from CLEA Japan, Inc.). All procedures involving animals and their care were approved by the Ethics Committee of Hokkaido University in accordance with institutional and Japanese government guidelines for animal experiments. Huh-7/Dlk cells (5×10^6 cells/animal) in 100 μL solution (PBS: Matrigel = 1: 1) were implanted s.c. into the back of mice. Matrigel was obtained from BD Biosciences. Tumor growth was monitored until it reached an acceptable size. For in vivo imaging, a 0.8-mL solution containing FBP-IgG or CLuc-IgG (25 ng/μL) was injected to mice intravenously. The same experiments were carried out twice. To obtain bioluminescence image, the mice were given injections of 100 μL of 2 μg/μL *Cypridina* luciferin at 24 h or 48 h. Bioluminescence imaging was performed by Photon Imager (Biospace Lab) equipped with an intensified CCD camera (18 mm diameter, objective lens: 24 mm, f/1.4–22) between 5 and 10 min after luciferin injection with 0.5-min exposure in the absence or in the presence of 570 nm long pass filter (30). In vivo fluorescence imaging was carried out just before luciferin injection using the same equipment with a Cy5 filter set (a 60-nanometer excitation pass band filter from 590 to 650 nanometers with a peak at 620 nm, and a 660 nanometers long-pass filter for the detection of emission) with 0.5-min exposure.

ACKNOWLEDGMENTS. This study was supported in part by a Grant-in-Aid for the Support of Young Researchers (grant no. 19710196 to C.W.), Grant-in-Aid (A) (grant no. 20249060 to M.O.) and Grant-in-Aid (C) (grant no. 19614002 to Y.O.) from the Ministry of Education, Culture, Sports, Science, and Technology, Japan. We thank Dr. S. Ohgiya (AIST) for his comments on the manuscript.

1. Adams R, Meade A, Wasan H, Griffiths G, Maughan T (2008) Cetuximab therapy in first-line metastatic colorectal cancer and intermittent palliative chemotherapy: Review of the COIN trial. *Expert Rev Anticancer Ther* 8:1237–1245.
2. Boltze J, et al. (2008) Permanent middle cerebral artery occlusion in sheep: A novel large animal model of focal cerebral ischemia. *J Cereb Blood Flow Metab* 28:1951–1964.
3. Ilowite NT (2008) Update on biologics in juvenile idiopathic arthritis. *Curr Opin Rheumatol* 20:613–618.
4. Menard C, et al. (2008) Ctla-4 blockade confers lymphocyte resistance to regulatory T-cells in advanced melanoma: Surrogate marker of efficacy of tremelimumab? *Clin* Cancer Res 14:5242–5249.
5. Wang Z, et al. (2008) Effect of rapamycin alone and in combination with sorafenib in an orthotopic model of human hepatocellular carcinoma. *Clin Cancer Res* 14:5124–5130.
6. Contag PR, Olomu IN, Stevenson DK, Contag CH (1998) Bioluminescent indicators in living mammals. *Nat Med* 4:245–247.
7. Hoffman RM, Yang M (2005) Dual-color, whole-body imaging in mice. *Nat Biotechnol* 23:790.
8. Ntziachristos V, Ripoll J, Wang LV, Weissleder R (2005) Looking and listening to light: The evolution of whole-body photonic imaging. *Nat Biotechnol* 23:313–320.
9. So MK, Xu C, Loening AM, Gambhir SS, Rao J (2006) Self-illuminating quantum dot conjugates for in vivo imaging. *Nat Biotechnol* 24:339–343.
10. Frangioni JV (2006) Self-illuminating quantum dots light the way. *Nat Biotechnol* 24:326–328.
11. Xu Y, Piston DW, Johnson CH (1999) A bioluminescence resonance energy transfer (BRET) system: Application to interacting circadian clock proteins. *Proc Natl Acad Sci USA* 96:151–156.
12. Shcherbo D, et al. (2007) Bright far-red fluorescent protein for whole-body imaging. *Nat Methods* 4:741–746.
13. Frangioni JV (2003) In vivo near-infrared fluorescence imaging. *Curr Opin Chem Biol* 7:626–634.
14. Shimomura O, Johnson FH (1971) Mechanism of the luminescent oxidation of *Cypridina* luciferin. *Biochem Biophys Res Commun* 44:340–346.
15. Thompson EM, Nagata S, Tsuji FI (1989) Cloning and expression of cDNA for the luciferase from the marine ostracod *Vargula hilgendorfii*. *Proc Natl Acad Sci USA* 86:6567–6571.
16. Nakajima Y, Kobayashi K, Yamagishi K, Enomoto T, Ohmiya Y (2004) cDNA cloning and characterization of a secreted luciferase from the luminous Japanese ostracod, *Cypridina noctiluca*. *Biosci Biotechnol Biochem* 68:565–570.
17. Shimomura O, Johnson FH, Saiga Y (1961) Purification and properties of *Cypridina* luciferase. *J Cell Comp Physiol* 58:113–123.
18. Shimomura O, Johnson FH, Masugi T (1969) *Cypridina* bioluminescence: Light-emitting oxyluciferin-luciferase complex. *Science* 164:1299–1300.
19. Wu C, et al. (2007) Preparation of biotinylated *Cypridina* luciferase and its use in bioluminescent enzyme immunoassay. *Anal Chem* 79:1634–1638.
20. Wu C, Kawasaki K, Ohgiya S, Ohmiya Y (2006) Syntheses and evaluation of the bioluminescent activity of (S)-*Cypridina* luciferin and its analogs. (Translated from English) *Tetrahedron Lett* 47:753–756.
21. Laborda J, Sausville EA, Hoffman T, Notario V (1993) dlk, a putative mammalian homeotic gene differentially expressed in small cell lung carcinoma and neuroendocrine tumor cell line. *J Biol Chem* 268:3817–3820.
22. Kogel D, et al. (2001) Dlk/ZIP kinase-induced apoptosis in human medulloblastoma cells: Requirement of the mitochondrial apoptosis pathway. *Br J Cancer* 85:1801–1808.
23. Tanimizu N, Nishikawa M, Saito H, Tsujimura T, Miyajima A (2003) Isolation of hepatoblasts based on the expression of Dlk/Pref-1. *J Cell Sci* 116:1775–1786.
24. Hsiao CC, et al. (2005) Differential expression of delta-like gene and protein in neuroblastoma, ganglioneuroblastoma and ganglioneuroma. *Mod Pathol* 18:656–662.
25. Dezso K, et al. (2008) Delta-like protein (DLK) is a novel immunohistochemical marker for human hepatoblastomas. *Virchows Arch* 452:443–448.
26. Schatz PJ (1993) Use of peptide libraries to map the substrate specificity of a peptide-modifying enzyme: A 13-residue consensus peptide specifies biotinylation in Escherichia coli. *Biotechnology* 11:1138–1143.
27. Nakajima Y, Kimura T, Suzuki C, Ohmiya Y (2004) Improved expression of novel red- and green-emitting luciferases of *Phrixothrix* railroad worms in mammalian cells. *Biosci Biotechnol Biochem* 68:948–951.
28. Venisnik KM, et al. (2006) Bifunctional antibody-*Renilla* luciferase fusion protein for in vivo optical detection of tumors. *Protein Eng Des Sel* 19:453–460.
29. Venisnik KM, Olafsen T, Gambhir SS, Wu AM (2007) Fusion of *Gaussia* luciferase to an engineered anti-carcinoembryonic antigen (CEA) antibody for in vivo optical imaging. *Mol Imaging Biol* 9:267–277.
30. Roncali E, et al. (2008) New device for real-time bioluminescence imaging in moving rodents. *J Biomed Opt* 13:054035.

Available online at www.sciencedirect.com
ScienceDirect
Leukemia Research 33 (2009) 151–158
Leukemia Research
www.elsevier.com/locate/leukres

Activation of c-Jun N-terminal kinase is essential for oxidative stress-induced Jurkat cell apoptosis by monochloramine

Tetsuya Ogino [a,*], Michitaka Ozaki [b], Mutsumi Hosako [a], Masako Omori [a], Shigeru Okada [a], Akihiro Matsukawa [a]

[a] *Pathology and Experimental Medicine, Okayama University Graduate School of Medicine, Dentistry and Pharmaceutical Sciences, 2-5-1 Shikata, Okayama 700-8558, Japan*

[b] *Department of Molecular Surgery, Hokkaido University Graduate School of Medicine, N-15, W-7, Kita-ku, Sapporo, Hokkaido 060-8638, Japan*

Received 23 March 2008; received in revised form 26 June 2008; accepted 10 July 2008
Available online 20 August 2008

Abstract

Leukemic cell apoptosis may be enhanced by appropriate oxidative stress. We report here the mechanism of Jurkat cell apoptosis by monochloramine (NH_2Cl), a neutrophil-derived oxidant. NH_2Cl induced caspase-dependent apoptosis, which was preceded by cytochrome *c* and Smac/Diablo release from mitochondria. Within 10 min of NH_2Cl treatment, c-Jun N-terminal kinase (JNK) activation and elevation of cytosolic Ca^{2+} were observed. JNK inhibitors (SP600125 or JNK inhibitor VIII) significantly suppressed the apoptosis as well as caspase cleavage and cytochrome *c* release. In contrast, Ca^{2+} chelation by EGTA + acetoxymethyl-EGTA had no effects on apoptosis. Our results indicated that JNK activation contributed most importantly to the NH_2Cl-induced apoptosis.

Keywords: Oxidative stress; Apoptosis; c-Jun N-terminal kinase; Chemotherapy; Mitochondria; Calcium

1. Introduction

Leukemia treatment largely depends on anticancer drugs, and oxidative stress is involved to a various extent in chemotherapy-induced apoptosis [1,2]. Oxidative stress is one of the effective apoptosis inducers and malignant cells are in general under intrinsic oxidative stress [3]. We have previously reported that multidrug-resistant NK tumor cell line underwent apoptosis by a neutrophil-derived oxidant monochloramine (NH_2Cl) [4]. Thus, leukemia therapy may be improved by properly modulating the oxidative stress of the tumor cells. However, exogenous oxidants sometimes disturb the effects of some chemotherapeutic drugs [5]. Thus, it is important to elucidate how oxidative stress induces or inhibits apoptosis of tumor cells.

NH_2Cl is produced by activated neutrophils in the reaction of OCl^- and NH_4^+ [6,7], and has various biological effects on signal transduction, gene expression, DNA repair and cell cycle [8–11]. NH_2Cl also induces apoptosis through the release of apoptosis-promoting proteins, such as cytochrome *c* and Smac/Diablo from mitochondria [4]. Cytochrome *c* promotes caspase 9 activation through the complex formation with apoptotic protease activating factor 1 [12], whereas Smac/Diablo suppresses inhibitor of apoptosis proteins that normally inhibit caspase activity [13,14]. Cytochrome *c* may be released through the opening of permeability transition pore [15,16], or by truncated Bid, a Bcl-2 family protein [17]. Notably, mitochondrial membrane potential decreases with the opening of permeability transition pore, whereas truncated Bid stimulates cytochrome *c* release without a decrease in mitochondrial membrane potential [18,19].

NH_2Cl causes several immediate cellular responses that can lead to cytochrome *c* release. Among them are Ca^{2+} increase in cytosol [20], p53 phosphorylation at Ser46 [10] and the activation of c-Jun N-terminal kinase (JNK). Experiments using isolated mitochondria showed that increase in

* Corresponding author. Tel.: +81 86 235 7145; fax: +81 86 235 7148.
E-mail address: togino@md.okayama-u.ac.jp (T. Ogino).

0145-2126/$ – see front matter © 2008 Elsevier Ltd. All rights reserved.
doi:10.1016/j.leukres.2008.07.009

cytosolic Ca^{2+} can induce mitochondrial membrane permeability transition and release cytochrome *c* [21]. Apoptosis can also be initiated by p53 phosphorylation, especially at S46 [22]. P53 may induce apoptosis by expressions of various genes, such as p53AIP1, NOXA, PUMA [23–25], or p53 may migrate to mitochondria and facilitate the release of apoptosis-promoting proteins probably through the interaction with Bcl-2 family proteins [26]. JNK is a member of MAP kinase family, and is activated by various stresses such as ultraviolet rays, heat shock, anticancer drugs, inflammatory cytokines and oxidative stress [27]. Although JNK may stimulate or inhibit apoptosis depending on the condition [28], it is reported that JNK stimulates TNFα-induced apoptosis by caspase 8 activation [29]. The goal of this study is to elucidate the link between these immediate cellular responses and the downstream apoptosis machinery. Our results indicated that JNK activation contributed most importantly to NH_2Cl-induced apoptosis.

2. Materials and methods

2.1. Reagents

Antibodies against caspases 2, 3, 8, Bid, Smac/Diablo, phospho-MKK4 (T261), phospho-JNK (T183/Y195), and phospho-ATF2 (T71) were from Cell Signaling Technology (Beverly, MA). Antibodies against MKK4 and JNK were from Transduction Laboratories (Lexington, KY), and cytochrome *c* was from BD PharMingen (San Diego, CA). Caspase inhibitors, namely Z-D(OMe)E(OMe)VD(OMe)-fmk (Z-DEVD-fmk) for caspase 3, Z-IE(OMe)TD(OMe)-fmk (Z-IETD-fmk) for caspase 8 and Z-LE(OMe)HD(OMe)-fmk (Z-LEHD-fmk) for caspase 9, JNK inhibitors, namely SP600125 (Anthra [1,9-*cd*] pyrazol-6(2H)-one) and JNK inhibitor VIII (*N*-(4-Amino-5-cyano-6-ethoxypyridin-2-yl)-2-(2,5-dimethoxyphenyl) acetamide), and hygromycin B were from Calbiochem (EMD Chemicals, San Diego, CA). Cyclosporin A was from Wako Pure Chemical (Osaka, Japan). Cycloheximide was from Sigma (St. Louis, MO). Monochloramine (NH_2Cl, about 5 mM) was prepared just before experiments and the concentration was measured by the UV absorption spectra as described previously [30]. All other reagents were of analytical grade or better.

2.2. Cell culture and treatment

Jurkat T cell, a human acute T cell leukemia cell line, was obtained from Hayashibara Biochemical Laboratories Inc. (Fujisaki Cell Center, Okayama, Japan). HL60 cell was from Health Science Research Resources Bank (Osaka, Japan). The cell culture medium was RPMI 1640 supplemented with 10% (v/v) fetal bovine serum, 2 mM L-glutamine, and 110 mg/l sodium pyruvate (from Life Technologies, Inc., Gaithersburg, MD, USA). Cells were cultured in a CO_2 incubator containing 5% CO_2 at 37 °C, and the cells in exponential growth phase were used for experiments.

For NH_2Cl pretreatment, cells were suspended in the fresh medium at 1×10^6 cells/ml. Where indicated, caspase inhibitors (final concentration at 25 μM each), JNK inhibitors (20 μM each), protein synthesis inhibitors (cycloheximide 5 μg/ml, hygromycin B 100 μg/ml) or Ca^{2+} chelating chemicals (EGTA 2 mM + EGTA-AM 50 μM) were added and incubated for 10–30 min as indicated in each figures. Then, 100 μM of NH_2Cl (i.e. 100 nmol/10^6 cells) were added and incubated for 10 min, 3 h or 6 h at 37 °C in a CO_2 incubator as described in the results. During the incubation time, even for 10 min, almost all NH_2Cl reacted with cells and medium components, and disappeared from the medium (data not shown). The treated cells were separated from the medium by centrifugation at 500 × *g* for 5 min, washed once with ice-cold PBS, and used for the following experiments.

2.3. Apoptosis detection

Apoptosis was detected by FITC-labeled annexin V and propidium iodide double staining method using TACS annexin V-FITC apoptosis detection kit (Trevigen, Gaithersburg, MD) and a flow cytometer (FACSCalibur, Becton Dickinson, Franklin Lakes, NJ). Cells stained with FITC-annexin V, but not with propidium iodide were considered apoptotic cells. Data were collected from a morphometrically homogeneous cell population, which typically contained more than 80% of cells.

2.4. Cell fractionation and Western blotting

Cytosolic and mitochondrial fractions were prepared immediately after cell harvest using mitochondria/cytosol fractionation kit (BioVision) according to manufacturer's instruction. The mitochondrial pellet was resuspended in lysis buffer consisting of 20 mM sodium phosphate buffer (pH 7.4) with phosphatase inhibitor cocktail (PhosStop, Roche, Mannheim, Germany), protease inhibitor cocktail (Complete mini, Roche) and 0.1% (v/v) Nonidet P-40. Whole cell protein was extracted in lysis buffer consisting of 20 mM sodium phosphate buffer (pH 7.4), 40 mM β-glycerophosphate, 20 mM NaF, 1 mM Na_3VO_4, 20 mM *p*-nitrophenyl phosphate, 1 mM dithiothreitol, 0.1% (v/v) Nonidet-P40, and protease inhibitor cocktail. The protein concentration was measured by Coomassie Plus Protein Assay Reagent (Pierce, Rockford, IL), and the same amount of protein was separated by SDS-PAGE and transferred to a PVDF membrane. Immunoreactive proteins were detected using chemiluminescence system (Nacalai, Kyoto, Japan).

2.5. Statistical analysis

For Western blot images, each band densities were measured using Image J software (http://rsb.info.nih.gov/ij/), and expressed as % of the sum of total band densities. Results were tabulated for the indicated number of experimental samples. Analysis of variance (ANOVA) was performed for multiple comparison using Statcel QC software (OMS publishing Inc., Saitama, Japan). The *P* values less than 0.05 were considered to be significantly different.

3. Results

3.1. NH_2Cl-induced apoptosis was caspase dependent

We first studied the caspase dependence of the NH_2Cl-induced apoptosis. NH_2Cl-induced apoptosis, which was

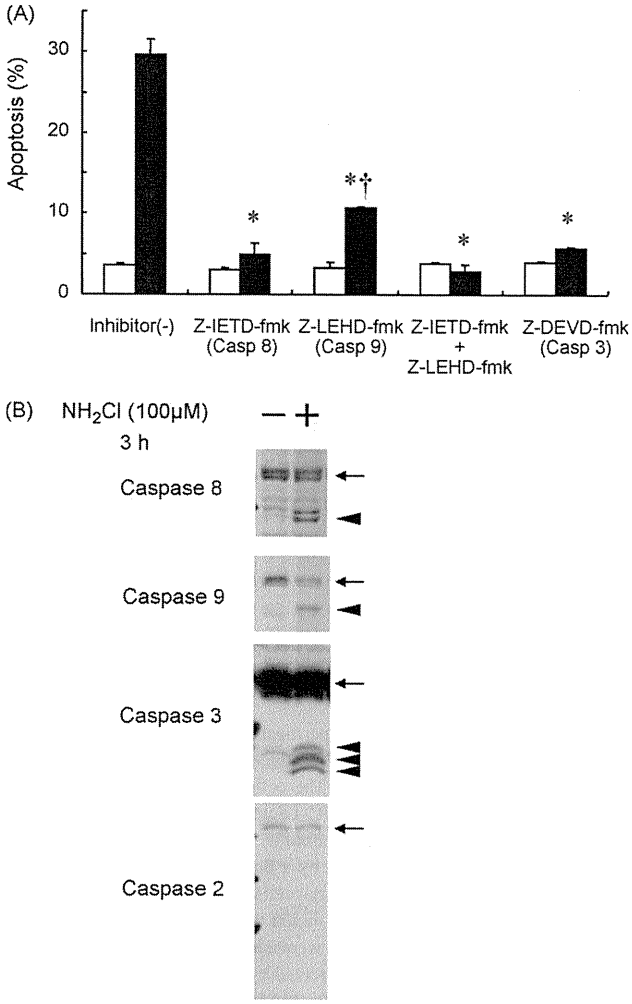

Fig. 1. NH_2Cl-induced apoptosis was caspase dependent. (A) Jurkat cells (suspended in a fresh culture medium at 1×10^6 cells/ml) were added with the indicated caspase inhibitors at 25 μM, and incubated for 30 min. Then the cells were added with 100 μM of NH_2Cl, and incubated for 6 h. Apoptosis was detected by annexin V method. Open bars: no NH_2Cl, closed bars: $NH_2Cl = 100$ μM. (*): Significantly lower than inhibitor (−), $NH_2Cl = 100$ μM samples. (†): Significantly higher than Z-IETD-fmk, $NH_2Cl = 100$ μM samples. Mean ± S.D. for three independent experiments. (B) Caspase cleavage was detected at 3 h after NH_2Cl (100 μM) addition. Whole cell lysate was prepared and analyzed by Western blotting. The same amount of protein was loaded on each well. Arrow: full-length caspase, arrowhead: cleaved caspases. Representative data from three independent experiments.

measured at 6 h of incubation, was almost completely inhibited by caspase 8 inhibitor (Z-IETD-fmk) or caspase 3 inhibitor (Z-DEVD-fmk) (Fig. 1A). Caspase 9 inhibitor (Z-LEHD-fmk), on the other hand, also showed a significant but partial inhibition. Combination of Z-IETD-fmk and Z-LEHD-fmk resulted in virtually complete inhibition.

Caspase cleavage was studied at 3 h after NH_2Cl treatment, when apoptotic cells were beginning to increase [31]. As expected, caspases 8 and 9 showed a definite cleavage, which indicated their activation (Fig. 1B). Caspase 3, a major execution caspase, also showed slight but definite cleavage, which also indicated its activation. Caspase 2 did not show apparent cleavage.

Caspase 8 can either directly activate caspase 3, or through mitochondrial pathway, which include Bid cleavage, cytochrome *c* release and caspase 9 activation [32]. Thus, the Bid cleavage and the release of apoptosis-inducing proteins from mitochondria were studied. After 3 h of NH_2Cl addition, truncated Bid was detectable especially in mitochondrial fraction (Fig. 2A). At the same time, cytochrome *c* and Smac/Diablo, which normally localize in mitochondria, appeared in the cytosolic fraction. To confirm that this Bid cleavage was catalyzed by caspase 8, the effects of Z-IETD-fmk was studied. Fig. 2B showed that Z-IETD-fmk almost completely inhibited Bid cleavage, as well as caspase 8 cleavage itself. The result indicated that Bid cleavage was catalyzed by caspase 8, and caspase 8 activated itself.

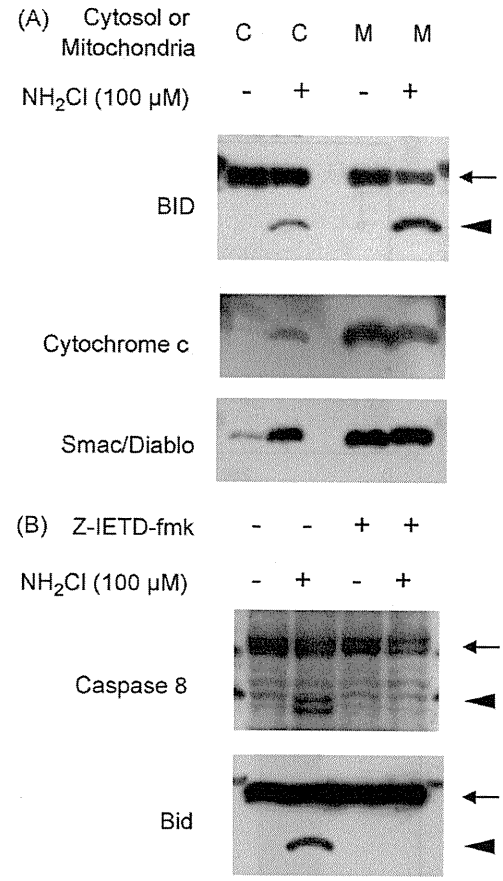

Fig. 2. NH_2Cl induced Bid cleavage and cytochrome *c* release. (A) Jurkat cells were added with 100 μM of NH_2Cl, and incubated for 3 h. Cell fractions were prepared using Mitochondria/Cytosol fractionation kit (BioVision) and analyzed by Western blotting. For cytosol and mitochondria samples, 5.1 and 8.6 μg of protein was loaded on each well, respectively. Arrow: full-length Bid, arrowhead: truncated Bid. Representative data from three independent experiments. (B) Jurkat cells were added with caspase 8 inhibitor (Z-IETD-fmk) at 25 μM, and incubated for 30 min. Then the cells were added with 100 μM of NH_2Cl, and incubated for 3 h. Whole cell lysate was prepared and analyzed by Western blotting. The same amount of protein was loaded on each well. Arrow: full-length proteins, arrowhead: cleaved proteins. Representative data from three independent experiments.

3.2. Cytosolic Ca^{2+} increased by NH_2Cl, but had no effects on apoptosis

It has been reported that increase in the cytosolic Ca^{2+} stimulated mitochondrial cytochrome *c* release by enhancing membrane permeability transition [33]. NH_2Cl addition to Jurkat cells resulted in immediate and sustained increase in the cytosolic Ca^{2+}, which was detected by the fluorescence of calcium indicator Fluo-3 (Fig. 3A). However, when extracellular and cytosolic Ca^{2+} was chelated by EGTA + acetoxymethyl-EGTA, NH_2Cl-induced apoptosis did not decrease (Fig. 3B). The classical membrane permeability transition shows the decrease in mitochondrial membrane potential and this phenomenon can be inhibited by cyclosporin A [34]. When the mitochondrial membrane potential was measured by JC-1 fluorescence, the cells with low membrane potential was only 9.2% even at 6 h after NH_2Cl addition, when the apoptotic cells were more than 20% (Fig. 4A and B). Consistent with this result, cyclosporin A pretreatment failed to inhibit NH_2Cl-induced apoptosis

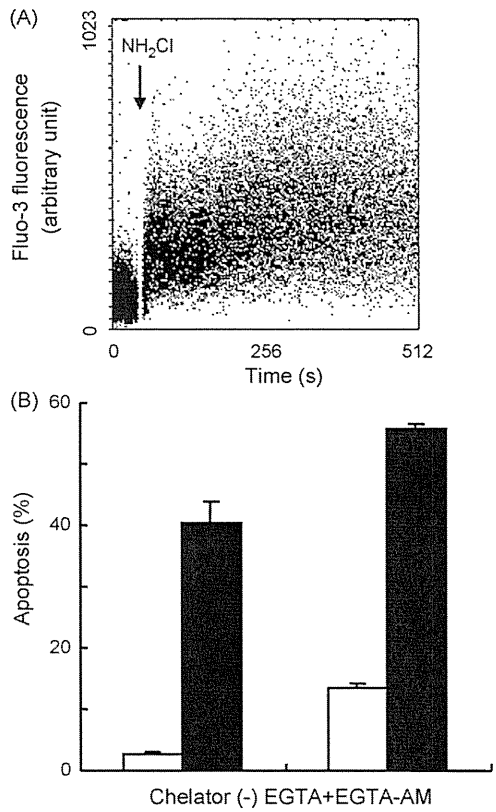

Fig. 3. Cytosolic Ca^{2+} elevation had no effects on apoptosis. (A) Jurkat cells (suspended in a fresh medium without phenol red at 1×10^6 cells/ml) were added with acetoxymethyl-Fluo3 at 2 μM, and incubated for 30 min. Flow cytometric analysis was started and 100 μM of NH_2Cl was added at 40 s (arrow), and the analysis was continued for up to 512 s. Representative data from three independent experiments. (B) Jurkat cells were added with EGTA (2 mM) and acetoxymethyl-EGTA (50 μM) and incubated for 30 min. Then the cells were added with 100 μM of NH_2Cl, and incubated for 6 h. Apoptosis was detected by annexin V method. Open bars: no NH_2Cl, closed bars: NH_2Cl = 100 μM. Mean ± S.D. for three independent experiments.

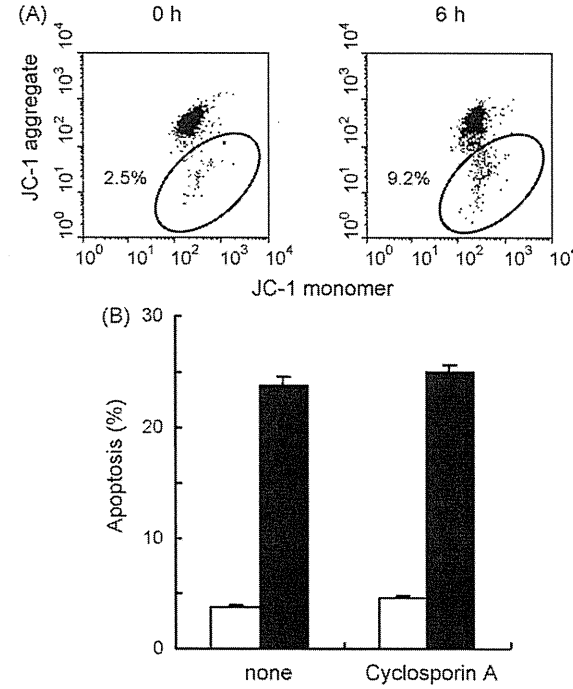

Fig. 4. Mitochondrial membrane permeability transition did not precede the apoptosis. (A) Jurkat cells were added with 100 μM of NH_2Cl, and incubated for the indicated times. The cells were washed, resuspended in PBS, and added with 2 μM of JC-1. JC-1 aggregate (high membrane potential cells, red fluorescence) and JC-1 monomer (low membrane potential cells, green fluorescence) were analyzed by a flow cytometer. Events inside the oval represent low membrane potential cells. Representative data from three experiments. (B) Jurkat cells were added with cyclosporin A at 1 μM and incubated for 10 min. Then the cells were added with 100 μM of NH_2Cl, and incubated for 6 h. Apoptosis was detected by annexin V method. Open bars: no NH_2Cl, closed bars: NH_2Cl = 100 μM Mean ± S.D. for three independent experiments.

(Fig. 4B). These results indicated that the classical membrane permeability transition was not involved in this apoptosis.

3.3. JNK inhibitors significantly inhibited NH_2Cl-induced apoptosis

NH_2Cl addition induced a rapid phosphorylation of JNK at T183/Y185, which was detectable at 4 min and the phosphorylation increased at 6 and 10 min (Fig. 5). The upstream kinase MKK4 and the downstream transcription factor ATF2 were also phosphorylated at the same time points, which indicated that JNK signaling pathway was activated by NH_2Cl. As JNK pathway is reported to be involved in TNFα-stimulated apoptosis [29], the role of JNK in NH_2Cl-induced apoptosis was studied using Jurkat cells and HL60 cells. In Jurkat cells, both of two different JNK inhibitors, namely SP600125 and JNK inhibitor VIII, inhibited NH_2Cl-induced apoptosis significantly, although not completely (Fig. 6A). Similar result was obtained using HL60 cells, in which JNK inhibitor VIII induced a significant but incomplete inhibition of NH_2Cl-induced apoptosis (Fig. 6B). The effects of JNK inhibition on caspase 8, Bid, cytochrome *c* and Smac/Diablo

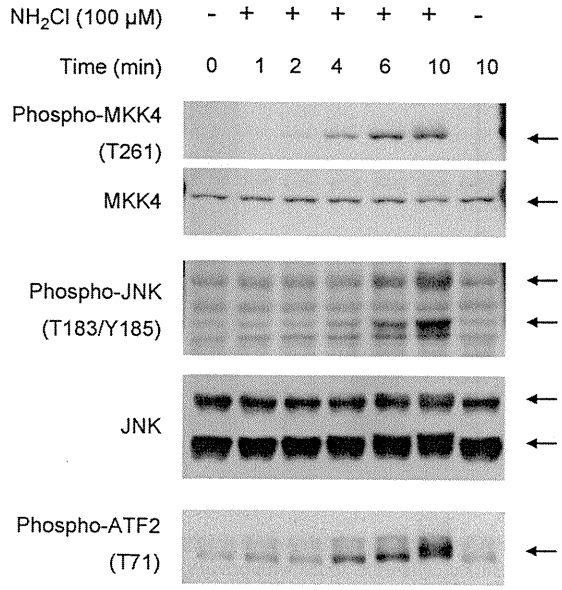

Fig. 5. JNK pathway was activated by NH_2Cl. Jurkat cells were added with 100 μM of NH_2Cl, and incubated for the indicated times. Whole cell lysate was prepared and the same amount of protein was analyzed by Western blotting using phospho-specific antibodies. As for MKK4 and JNK, the same membrane was stripped and reprobed using each protein-specific antibodies. Representative data from three independent experiments.

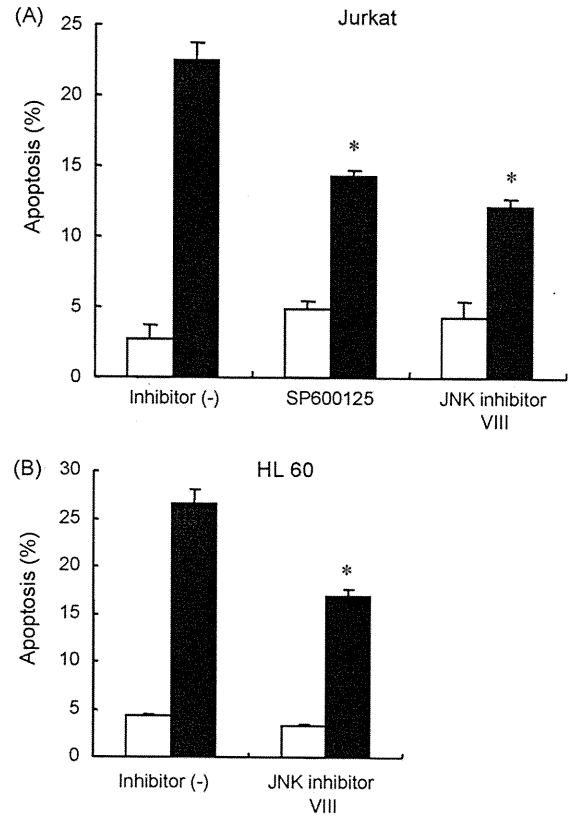

Fig. 6. JNK inhibitors significantly inhibited NH_2Cl-induced apoptosis. (A) Jurkat cells were added with the indicated JNK inhibitors at 20 μM, and incubated for 10 min. Then the cells were added with 100 μM of NH_2Cl, and incubated for 6 h. Apoptosis was detected by annexin V method. (B) The same experiment was done using HL60 cells. Open bars: no NH_2Cl, closed bars: NH_2Cl = 100 μM. (*): Significantly decreased from inhibitor (−), NH_2Cl = 100 μM samples. Mean ± S.D. for at least three independent experiments.

were also studied. Caspase 8 and Bid cleavage were clearly inhibited by a JNK inhibitor SP600125 (Fig. 7). The release of cytochrome *c* and Smac/Diablo were also inhibited significantly.

JNK-mediated apoptosis may require a new protein synthesis [35], thus, the effects of protein synthesis inhibitors were studied. NH_2Cl-induced apoptosis was not inhibited but rather enhanced by protein synthesis inhibitors (Fig. 8), which indicated that new protein synthesis was not a prerequisite for this apoptosis.

3.4. NH_2Cl induced p53(Ser46) phosphorylation and migration to mitochondria

NH_2Cl is reported to enhance p53 phosphorylation at Ser46 [10]. As Ser46 phosphorylation of p53 is linked to apoptosis [23], the role of p53 in NH_2Cl-induced apoptosis was studied. NH_2Cl treatment induced a rapid p53 phosphorylation at Ser46 within 10 min (Fig. 9A). Interestingly, mitochondria-associated p53 increased significantly after 3 h of NH_2Cl treatment (Fig. 9B).

4. Discussion

In this paper we studied the mechanism of NH_2Cl-induced apoptosis in Jurkat cells. From the experiments, the probable apoptosis pathways were shown in Fig. 10, and the most important pathway included JNK phosphorylation, caspase 8 activation, Bid cleavage, cytochrome *c* and Smac/Diablo release from mitochondria, caspase 9 activation and caspase 3 activation. Caspase 8 may also activate caspase 3 directly. In addition, p53 migration to mitochondria may also stimulate cytochrome *c* release. Although cytosolic Ca^{2+} increased immediately after NH_2Cl treatment, it had no effects on apoptosis.

Although exogenous oxidants disturb chemotherapeutic drugs in some conditions [5], applying oxidative stress to chemotherapy has certain advantages, i.e., cancer cells are more preferentially damaged than normal cells [3], and multidrug-resistant cells can also be damaged by oxidants [4]. As these apparently conflicting results may be explained by the difference in the types, doses or targets of oxidants, the detailed mechanism of oxidant action needs to be elucidated. In the case of NH_2Cl-induced apoptosis, JNK activation appeared to be necessary. In addition to Jurkat cells, HL60 cells also showed inhibition of NH_2Cl-induced apoptosis by JNK inhibitor VIII. When the phosphorylation of MKK4, JNK and ATF2 were compared at various time points, they were phosphorylated almost simultaneously after NH_2Cl addition. Reactive oxygen species has been reported to activate JNK, which may be due to the decrease of JNK phosphatase, a member of MAP kinase phosphatase, in its

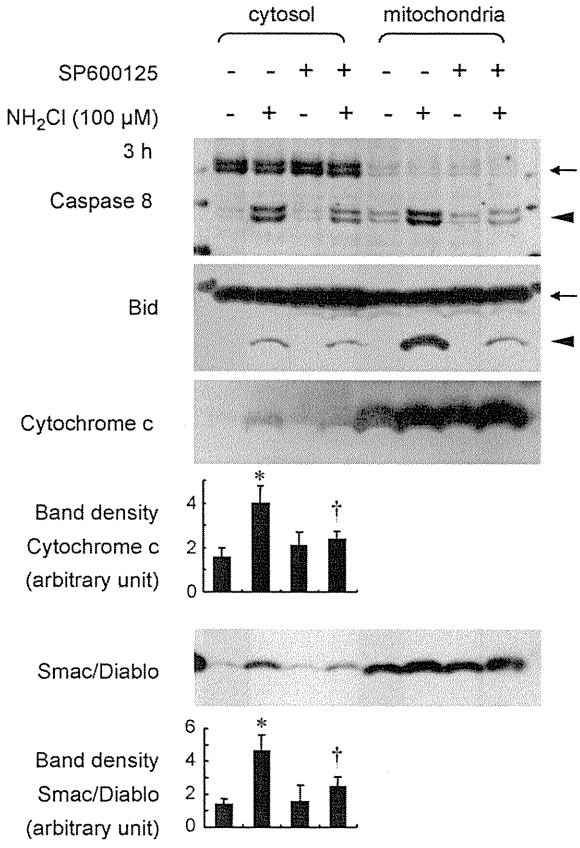

Fig. 7. The JNK inhibitor attenuated caspase 8 activation, Bid cleavage and cytochrome *c* release. Jurkat cells were added with JNK inhibitor (SP600125) at 20 μM, and incubated for 10 min. Then the cells were added with 100 μM of NH_2Cl, and incubated for 3 h. Cell fractions were prepared using Mitochondria/Cytosol fractionation kit (BioVision) and analyzed by Western blotting. For cytosol and mitochondria samples, 11.2 and 9.8 μg of protein was loaded on each well, respectively. Arrow: full-length proteins, arrowhead: cleaved proteins. The band densities of cytochrome *c* and Smac/Diablo were measured and analyzed by ANOVA. (*): Significantly higher than SP600125 (−), NH_2Cl (−) samples, (†): significantly lower than SP600125 (−), NH_2Cl (100 μM) samples, Representative data from three independent experiments.

expression level [36] or its enzyme activity [37]. MAP kinase phosphatase has a conserved catalytic cysteine residue, and its oxidation to sulfenic acid inactivates the enzyme [37]. As NH_2Cl preferentially oxidizes SH group [38], it is likely that NH_2Cl inactivated JNK phosphatase. This assumption is consistent with the observed rapid activation JNK pathway.

JNK inhibitor SP600125 suppressed caspase 8 cleavage, which indicated that active JNK facilitates caspase 8 activation. Recent report suggested that the degradation of FLICE-inhibitory protein (FLIP), one of the endogenous caspase inhibitor proteins, was facilitated by active JNK. JNK phosphorylates and activates Itch, a c-FLIP-specific E3 ubiquitin ligase, and promotes c-FLIP degradation [29]. We also studied the amount of FLIP after NH_2Cl treatment, which did not show definite changes (data not shown). In addition, Jurkat cells generally have rather low levels of FLIP protein. Thus, it should be studied further if FLIP degradation is involved in NH_2Cl-induced apoptosis.

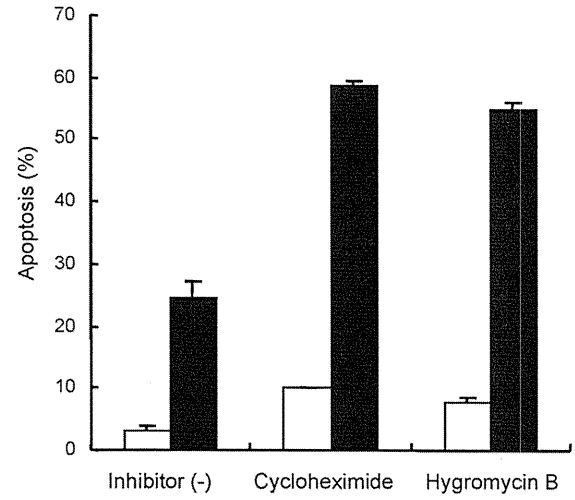

Fig. 8. NH_2Cl-induced apoptosis was not inhibited by protein synthesis inhibitors. Jurkat cells were added with protein synthesis inhibitors (cycloheximide at 5 μg/ml, hygromycin B at 100 μg/ml) and incubated for 10 min. Then the cells were added with 100 μM of NH_2Cl, and incubated for 6 h. Apoptosis was detected by annexin V method. Open bars: no NH_2Cl, closed bars: NH_2Cl = 100 μM. Mean ± S.D. for three independent experiments.

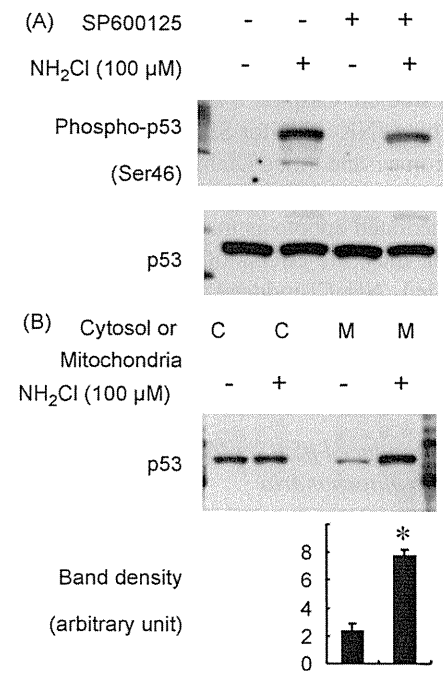

Fig. 9. NH_2Cl enhanced p53(S46) phosphorylation and migration to mitochondria. (A) Jurkat cells were added with JNK inhibitor (SP600125) at 20 μM, and incubated for 10 min. Then the cells were added with 100 μM of NH_2Cl, and incubated for 10 min. Whole cell lysate was prepared and the same amount of protein was analyzed by Western blotting using phospho-specific p53(Ser46) antibody. The same membrane was stripped and reprobed using protein-specific p53 antibody. Representative data from three independent experiments. (B) Jurkat cells were added with 100 μM of NH_2Cl, and incubated for 3 h. Cell fractions were prepared using Mitochondria/Cytosol fractionation kit (BioVision) and analyzed by Western blotting. For cytosol and mitochondria samples, 5.1 and 8.6 μg of protein was loaded on each well, respectively. The band densities of p53 in mitochondria were measured and analyzed by Student's *t*-test. (*): Significantly higher than NH_2Cl (−) sample. Representative data from three independent experiments.

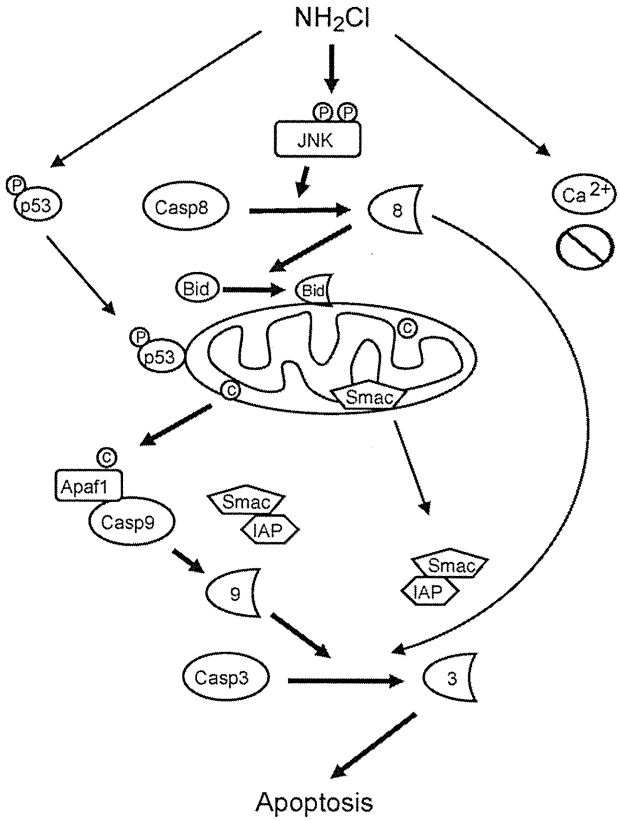

Fig. 10. Schematic drawing of the NH_2Cl-induced apoptosis pathway. The bold arrows indicate the major pathway. The increase in the cytosolic Ca^{2+} had no effects on apoptosis.

The apoptosis inhibition by JNK inhibitors was not complete. One possibility is that the JNK inhibition was not complete. Previous reports showed that slight JNK activity still remained at 20 μM of SP600125 [39,40]. Nevertheless, this concentration was chosen in this experiment because the higher concentration may inactivate other kinases [39]. It is also possible that there is an additional pathway that activates caspase. In this respect, p53 migration to mitochondria is a notable finding. It has been reported that p53 migration to mitochondria is sufficient to induce cytochrome *c* release [41]. The migrated p53 may interact with Bcl-2 family proteins and facilitates cytochrome *c* release [41]. Thus, it is plausible that the observed p53 migration may also stimulate cytochrome *c* release. P53 may also stimulate apoptosis through the induction of apoptosis-enhancing proteins [23]. Consistent with our previous report [10], NH_2Cl induced p53(Ser46) phosphorylation in Jurkat cells, and this phosphorylation is reported to enhance the expression of apoptosis-related genes [42]. However, the NH_2Cl-induced apoptosis was not inhibited by protein synthesis inhibitors, instead, the apoptosis was rather enhanced. Cycloheximide is reported to enhance apoptosis induced by Fas or tumor necrosis factor-α [43,44]. In these conditions, cycloheximide preferentially decreased apoptosis-inhibiting proteins, such as FLIP, X-linked inhibitor of apoptosis protein, and cellular inhibitor of apoptosis protein. Thus, the enhancement of apoptosis by cycloheximide in our experiment may be explained by the decrease in these apoptosis-inhibiting proteins. Therefore, it needs to be studied further if p53-dependent gene expression was involved in NH_2Cl-induced apoptosis.

In this experiment, it became clear that JNK activation was primarily important in the oxidative stress-induced apoptosis by NH_2Cl. It has been reported that JNK activation and generation of reactive oxygen species is important in the action of several therapeutic drugs, such as tyrosine kinase inhibitor + proteasome inhibitor [45] and As_2O_3 [46]. In these cases chloramine and the therapeutic drugs may enhance apoptosis cooperatively, because they work through similar pathways. If oxidative stress by chloramine is applicable adequately, we may be able to decrease the dose of anticancer drugs, thereby reducing side effects without loss of anticancer efficacy. Thus, it is an interesting future subject if we can properly modify tumor cell oxidative stress by exogenous oxidants and improve therapeutic protocols.

Conflict of interest

MH is a recipient of a grant from the Japan Leukemia Research Fund.

Acknowledgment

This study was supported by the Program for Promotion of Fundamental Studies in Health Sciences of the National Institute of Biomedical Innovation (NIBIO).

References

[1] Conklin KA. Cancer chemotherapy and antioxidants. J Nutr 2004;134:3201S–4S.
[2] Gokhale P, Patel T, Morrison MJ, Vissers MC. The effect of intracellular ascorbate on the susceptibility of HL60 and Jurkat cells to chemotherapy agents. Apoptosis 2006;11:1737–46.
[3] Hileman EO, Liu J, Albitar M, Keating MJ, Huang P. Intrinsic oxidative stress in cancer cells: a biochemical basis for therapeutic selectivity. Cancer Chemother Pharmacol 2004;53:209–19.
[4] Than TA, Ogino T, Hosako M, Omori M, Tsuchiyama J, Okada S. Physiological oxidants induce apoptosis and cell cycle arrest in a multidrug-resistant natural killer cell line, NK-YS. Leuk Lymphoma 2003;44:2109–16.
[5] Shacter E, Williams JA, Hinson RM, Senturker S, Lee YJ. Oxidative stress interferes with cancer chemotherapy: inhibition of lymphoma cell apoptosis and phagocytosis. Blood 2000;96:307–13.
[6] Grisham MB, Jefferson MM, Melton DF, Thomas EL. Chlorination of endogenous amines by isolated neutrophils. Ammonia-dependent bactericidal, cytotoxic, and cytolytic activities of the chloramines. J Biol Chem 1984;259:10404–13.
[7] Weiss SJ, Lampert MB, Test ST. Long-lived oxidants generated by human neutrophils: characterization and bioactivity. Science 1983;222:625–8.
[8] Ogino T, Kobuchi H, Sen CK, Roy S, Packer L, Maguire JJ. Monochloramine inhibits phorbol ester-inducible neutrophil respiratory burst

activation and T cell interleukin-2 receptor expression by inhibiting inducible protein kinase C activity. J Biol Chem 1997;272:26247–52.
[9] Omori M, Ogino T, Than TA, Okada S. Monochloramine inhibits the expression of E-selectin and intercellular adhesion molecule-1 induced by TNF-α through the suppression of NF-κB activation in human endothelial cells. Free Radic Res 2002;36:845–52.
[10] Hiramatsu K, Ogino T, Ozaki M, Okada S. Monochloramine inhibits ultraviolet B-induced p53 activation and DNA repair response in human fibroblasts. Biochim Biophys Acta 2006;1763:188–96.
[11] Hosako M, Ogino T, Omori M, Okada S. Cell cycle arrest by monochloramine through the oxidation of retinoblastoma protein. Free Radic Biol Med 2004;36:112–22.
[12] Zou H, Li Y, Liu X, Wang X. An APAF-1.cytochrome *c* multimeric complex is a functional apoptosome that activates procaspase-9. J Biol Chem 1999;274:11549–56.
[13] Du C, Fang M, Li Y, Li L, Wang X. Smac, a mitochondrial protein that promotes cytochrome *c*-dependent caspase activation by eliminating IAP inhibition. Cell 2000;102:33–42.
[14] Verhagen AM, Ekert PG, Pakusch M, Silke J, Connolly LM, Reid GE, et al. Identification of DIABLO, a mammalian protein that promotes apoptosis by binding to and antagonizing IAP proteins. Cell 2000;102:43–53.
[15] Bradham CA, Qian T, Streetz K, Trautwein C, Brenner DA, Lemasters JJ. The mitochondrial permeability transition is required for tumor necrosis factor α-mediated apoptosis and cytochrome *c* release. Mol Cell Biol 1998;18:6353–64.
[16] Crompton M, Barksby E, Johnson N, Capano M. Mitochondrial intermembrane junctional complexes and their involvement in cell death. Biochimie 2002;84:143–52.
[17] Esposti MD. The roles of Bid. Apoptosis 2002;7:433–40.
[18] Smaili SS, Hsu YT, Youle RJ, Russell JT. Mitochondria in Ca^{2+} signaling and apoptosis. J Bioenerg Biomembr 2000;32:35–46.
[19] Shimizu S, Tsujimoto Y. Proapoptotic BH3-only Bcl-2 family members induce cytochrome *c* release, but not mitochondrial membrane potential loss, and do not directly modulate voltage-dependent anion channel activity. Proc Natl Acad Sci U S A 2000;97:577–82.
[20] Cima RR, Dubach JM, Wieland AM, Walsh BM, Soybel DI. Intracellular Ca^{2+} and Zn^{2+} signals during monochloramine-induced oxidative stress in isolated rat colon crypts. Am J Physiol Gastrointest Liver Physiol 2006;290:G250–61.
[21] Kanno T, Sato EE, Muranaka S, Fujita H, Fujiwara T, Utsumi T, et al. Oxidative stress underlies the mechanism for Ca^{2+}-induced permeability transition of mitochondria. Free Radic Res 2004;38:27–35.
[22] D'Orazi G, Cecchinelli B, Bruno T, Manni I, Higashimoto Y, Saito S, et al. Homeodomain-interacting protein kinase-2 phosphorylates p53 at Ser 46 and mediates apoptosis. Nat Cell Biol 2002;4:11–9.
[23] Oda K, Arakawa H, Tanaka T, Matsuda K, Tanikawa C, Mori T, et al. p53AIP1, a potential mediator of p53-dependent apoptosis, and its regulation by Ser-46-phosphorylated p53. Cell 2000;102:849–62.
[24] Yakovlev AG, Di Giovanni S, Wang G, Liu W, Stoica B, Faden AI. BOK and NOXA are essential mediators of p53-dependent apoptosis. J Biol Chem 2004;279:28367–74.
[25] Jeffers JR, Parganas E, Lee Y, Yang C, Wang J, Brennan J, et al. Puma is an essential mediator of p53-dependent and -independent apoptotic pathways. Cancer Cell 2003;4:321–8.
[26] Moll UM, Wolff S, Speidel D, Deppert W. Transcription-independent pro-apoptotic functions of p53. Curr Opin Cell Biol 2005;17:631–6.
[27] Kyriakis JM, Avruch J. Mammalian mitogen-activated protein kinase signal transduction pathways activated by stress and inflammation. Physiol Rev 2001;81:807–69.
[28] Liu J, Lin A. Role of JNK activation in apoptosis: a double-edged sword. Cell Res 2005;15:36–42.
[29] Chang L, Kamata H, Solinas G, Luo JL, Maeda S, Venuprasad K, et al. The E3 ubiquitin ligase itch couples JNK activation to TNFα-induced cell death by inducing c-FLIP(L) turnover. Cell 2006;124:601–13.
[30] Thomas EL, Grisham MB, Jefferson MM. Preparation and characterization of chloramines. Methods Enzymol 1986;132:569–85.
[31] Ogino T, Ma Y, Than TA, Omori M, Okada S. Monochloramine enhances Fas (APO-1/CD95)-induced apoptosis in Jurkat T cells. J Leukoc Biol 2000;67:46–52.
[32] Li H, Zhu H, Xu CJ, Yuan J. Cleavage of BID by caspase 8 mediates the mitochondrial damage in the Fas pathway of apoptosis. Cell 1998;94:491–501.
[33] Szalai G, Krishnamurthy R, Hajnoczky G. Apoptosis driven by IP(3)-linked mitochondrial calcium signals. EMBO J 1999;18:6349–61.
[34] Kanno T, Fujita H, Muranaka S, Yano H, Utsumi T, Yoshioka T, et al. Mitochondrial swelling and cytochrome *c* release: sensitivity to cyclosporin A and calcium. Physiol Chem Phys Med NMR 2002;34:91–102.
[35] Atfi A, Buisine M, Mazars A, Gespach C. Induction of apoptosis by DPC4, a transcriptional factor regulated by transforming growth factor-beta through stress-activated protein kinase/c-Jun N-terminal kinase (SAPK/JNK) signaling pathway. J Biol Chem 1997;272:24731–4.
[36] Chen YR, Shrivastava A, Tan TH. Down-regulation of the c-Jun N-terminal kinase (JNK) phosphatase M3/6 and activation of JNK by hydrogen peroxide and pyrrolidine dithiocarbamate. Oncogene 2001;20:367–74.
[37] Kamata H, Honda S, Maeda S, Chang L, Hirata H, Karin M. Reactive oxygen species promote TNFα-induced death and sustained JNK activation by inhibiting MAP kinase phosphatases. Cell 2005;120:649–61.
[38] Peskin AV, Winterbourn CC. Kinetics of the reactions of hypochlorous acid and amino acid chloramines with thiols, methionine, and ascorbate. Free Radic Biol Med 2001;30:572–9.
[39] Bennett BL, Sasaki DT, Murray BW, O'Leary EC, Sakata ST, Xu W, et al. SP600125, an anthrapyrazolone inhibitor of Jun N-terminal kinase. Proc Natl Acad Sci U S A 2001;98:13681–6.
[40] Han Z, Boyle DL, Chang L, Bennett B, Karin M, Yang L, et al. c-Jun N-terminal kinase is required for metalloproteinase expression and joint destruction in inflammatory arthritis. J Clin Invest 2001;108:73–81.
[41] Mihara M, Erster S, Zaika A, Petrenko O, Chittenden T, Pancoska P, et al. p53 has a direct apoptogenic role at the mitochondria. Mol Cell 2003;11:577–90.
[42] Di Stefano V, Rinaldo C, Sacchi A, Soddu S, D'Orazi G. Homeodomain-interacting protein kinase-2 activity and p53 phosphorylation are critical events for cisplatin-mediated apoptosis. Exp Cell Res 2004;293:311–20.
[43] Fulda S, Meyer E, Debatin KM. Metabolic inhibitors sensitize for CD95 (APO-1/Fas)-induced apoptosis by down-regulating Fas-associated death domain-like interleukin 1-converting enzyme inhibitory protein expression. Cancer Res 2000;60:3947–56.
[44] Mitsiades N, Mitsiades CS, Poulaki V, Anderson KC, Treon SP. Intracellular regulation of tumor necrosis factor-related apoptosis-inducing ligand-induced apoptosis in human multiple myeloma cells. Blood 2002;99:2162–71.
[45] Dasmahapatra G, Rahmani M, Dent P, Grant S. The tyrphostin adaphostin interacts synergistically with proteasome inhibitors to induce apoptosis in human leukemia cells through a reactive oxygen species (ROS)-dependent mechanism. Blood 2006;107:232–40.
[46] Chen D, Chan R, Waxman S, Jing Y. Buthionine sulfoximine enhancement of arsenic trioxide-induced apoptosis in leukemia and lymphoma cells is mediated via activation of c-Jun NH_2-terminal kinase and up-regulation of death receptors. Cancer Res 2006;66:11416–23.

Biochemical and Biophysical Research Communications 380 (2009) 844–849

Contents lists available at ScienceDirect

Biochemical and Biophysical Research Communications

journal homepage: www.elsevier.com/locate/ybbrc

In vivo bioluminescence imaging of bone marrow-derived cells in brain inflammation

Hidetoshi Akimoto [a], Hyuck Joon Kwon [b], Michitaka Ozaki [c], Kazunori Yasuda [b], Ken-ichi Honma [d], Yoshihiro Ohmiya [a,*]

[a] Department of Photobiology, Research Center for Cooperative Projects, Hokkaido University Graduate School of Medicine, N-15, W-7, Kita-ku, Sapporo 060-0810, Japan
[b] Department of Sports Medicine and Joint Surgery, Hokkaido University Graduate School of Medicine, N-15, W-7, Kita-ku, Sapporo 060-0810, Japan
[c] Department of Molecular Surgery, Hokkaido University Graduate School of Medicine, N-15, W-7, Kita-ku, Sapporo 060-0810, Japan
[d] Department of Physiology, Hokkaido University Graduate School of Medicine, N-15, W-7, Kita-ku, Sapporo 060-0810, Japan

ARTICLE INFO

Article history:
Received 21 January 2009
Available online 5 February 2009

Keywords:
Bone marrow-derived cells
Brain inflammation
In vivo bioluminescence imaging

ABSTRACT

It has been accepted that bone marrow cells infiltrate the brain and play important roles in neuroinflammation. However, there is no good tool for the visualization of these cells in living animals. In this study, we generated mice that were transplanted with GFP- or luciferase-expressing bone marrow cells, and performed *in vivo* fluorescence imaging (FLI) and *in vivo* bioluminescence imaging (BLI) to visualize the infiltrated cells. Brain inflammation was induced by intrahippocampal injection of lipopolysaccharide (LPS). Immunohistochemical investigation demonstrated an increase in the infiltration of bone marrow cells into the hippocampus because of the LPS injection and differentiation of the infiltrated cells into microglia, but not into neurons or astrocytes. BLI, but not FLI, successfully detected an increase in signal intensity with the LPS injection, and the increase of BLI coincided with that of luciferase activity in hippocampus. BLI could quantitatively and continuously monitor bone marrow-derived cells *in vivo*.

It has recently become clear that bone marrow cells are able to cross the blood–brain barrier (BBB), infiltrate the CNS parenchyma, and differentiate into microglia (bone marrow-derived microglia) [1]. The bone marrow-derived microglia are particularly interesting because they could have direct implications for the etiology (physiopathology) of many neurodegenerative diseases, including stroke [2,3], traumatic brain injury [4,5], multiple sclerosis [6], Parkinson's disease [7], and Alzheimer's disease [8,9]. However, the precise role of these cells, beneficial or detrimental, is still under debate. Therefore, a monitoring system for bone marrow-derived microglia *in vivo* would contribute to provide valuable information about the role of microglia in neurodegenerative diseases.

Currently, the study of bone marrow-derived microglia is limited largely to histological investigation [1], because there is no good exogenous marker to distinguish resident microglia and bone marrow-derived microglia. Thus, producing a specific probe for only recognizing bone marrow-derived microglia, was extremely difficult. Even if the markers exist, the quantification and proliferation of the cells cannot be assessed easily *in vivo* because they are often degraded, diluted, and excreted as cell populations divide. On the other hand, *in vivo* optical techniques, such as fluorescence [10] and bioluminescence [11] are possibly powerful new modalities for the imaging of infiltrating bone marrow cells in the brain because GFP and luciferase are expressed in all cell progeny without dilution.

The overall goal of this study was to visualize bone marrow-derived microglia infiltrating the brain during neuroinflammation by *in vivo* optical imaging. To achieve this goal, we made transplanted bone marrow-derived microglia detectable in mice, by having them express GFP or firefly luciferase. Intrahippocampal lipopolysaccharide (LPS) injection was used for the induction of brain inflammation. Histological investigation demonstrated that bone marrow cells infiltrating the brain differentiated into microglia, but not into neurons or astrocytes. The bone marrow-derived microglia infiltrated mainly into the hippocampus and were serially and clearly visualized in living animals by *in vivo* bioluminescence imaging (BLI), but not *in vivo* fluorescent imaging (FLI).

Materials and methods

Animals. Twenty-four male C57 BL/6j mice (Clea Japan, Tokyo), 4 male EGFP transgenic mice (C57 BL/6j background) [12] as the donors of GFP-expressing bone marrow cells, and 4 male *mPer1*-luc transgenic mice (C57 BL/6j background) [13] as donors for luciferase-expressing bone marrow cells were used in the experiments. These mice were fed lab chow and kept under a 12 h light/dark cycle under SPF conditions in our animal facility. The animals were

* Corresponding author. Fax: +81 11 706 5042.
E-mail address: y-ohmiya@aist.go.jp (Y. Ohmiya).

0006-291X/$ - see front matter © 2009 Elsevier Inc. All rights reserved.
doi:10.1016/j.bbrc.2009.01.181

cared for according to the Guidelines for the Care and Use of Laboratory Animals at Hokkaido University Graduate School of Medicine.

Irradiation and bone marrow transplantation. Bone marrow cells of 8-week-old male GFP transgenic mice and luciferase transgenic mice of the same age, were aseptically harvested from their femurs and tibial cavities. Eight-week-old male C57BL/6J mice acted as recipients. They were exposed to 9 Gy total-body irradiation using a cobalt-60 source (MBR-150R2, Hitachi Medical, Tokyo, Japan). Eighteen hours later, the harvested GFP- or luciferase-expressing bone marrow cells were injected intravenously through a tail vein at a dose of 5×10^6 cells per individual. Irradiated mice transplanted with this suspension were housed in autoclaved cages under a 12 h light/dark cycle. Animals were used 3 months after the transplantation.

Stereotaxic surgery and intrahippocampal injections. Animals were anesthetized with isoflurane, and immobilized in stereotaxic apparatus (Narishige, Tokyo, Japan). Stereotaxic coordinates were −2.5 mm posterior, ±1.7 mm lateral, and −2.2 mm ventral from bregma. In this study, 1-μl injections of 4 μg/ul LPS (*Salmonella abortus equine*, Sigma, St. Louis, MO) dissolved in sterile saline were delivered over a 2-min period into each hippocampus. Control mice were injected with the saline alone. An approximately 10 mm diameter of scalp was resected to expose cranial bone and covered with dental enamel cement. The animals were then housed individually, and used for *in vivo* imaging at different time points (0, 1, 3, 5, or 7 days postinjection), and sacrificed at day 7 following the last imaging.

In vivo optical imaging. FLI was performed with an *in vivo* imaging system (Photon Imager, Biospace, France) with 10 s exposure and anesthetized with isoflurane during imaging. The same imaging system was used for BLI; mice were injected IP with 150 mg/kg D-luciferin (Wako, Osaka, Japan) 15 min before imaging and anesthetized with isoflurane during imaging. Photons emitted from living mice were acquired as photons per s/cm^2 per steradian by using Photon Vision + software version 1.0 (Biospace). For photon quantification, a region of interest (ROI) was manually selected and kept constant within all experiments. For longitudinal comparison of fluorescence or bioluminescence, baseline imaging was performed just before LPS administration. Each was expressed as a fold induction over baseline levels.

Brain tissue preparation. The mice were transcardially perfused with 30 ml of ice-cold heparinized (1 U/ml) saline to remove blood from their brains. The brain was quickly removed after decapitation and cut into two hemispheres on ice; the right brain hemispheres were used for subsequent biochemical analysis. The left hemispheres were fixed with a 4% neutral buffered paraformaldehyde solution for 24 h at 4 °C and cryoprotected with 30% sucrose in 0.1 M phosphate-buffered solution (pH 7.0) for 48 h at 4 °C. Coronal sections (30 μm thick) were cut with a freezing microtome. At least three animals were used for these studies.

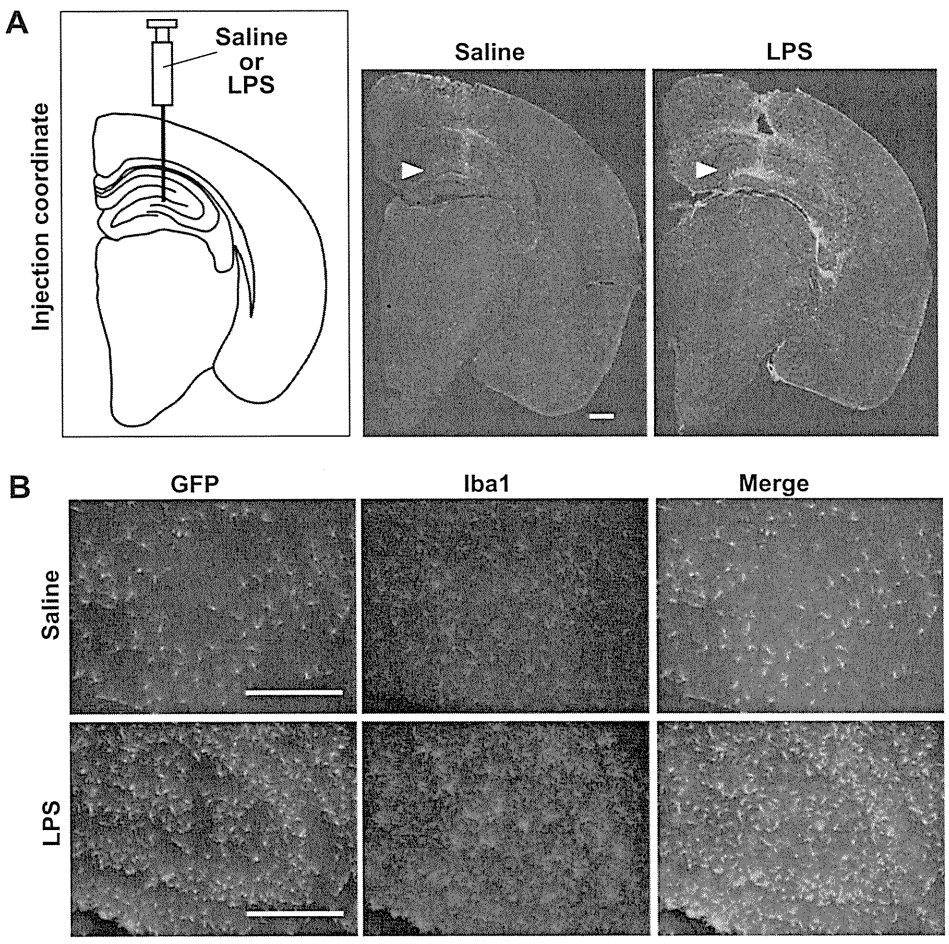

Fig. 1. Increased bone marrow-derived cells and brain inflammation in LPS-injected mice. (A) Panoramic view of a coronal section (left hemisphere) and coordination of intrahippocampal injection of saline or LPS. GFP-expressing bone marrow cells (green) increased in LPS injected brain. Scale bar = 500 μm. (B) Example of infiltrated GFP-expressing cells in a region of hippocampus. Increased bone marrow-derived cells (GFP in green) and upregulated brain inflammation (Iba1 in red) was observed in LPS-injected brain. Scale bars = 200 μm.

Immunohistochemistry. Free-floating sections were washed with Phosphate buffer saline (PBS) containing 0.05% Tween 100 (PBST) and were incubated for 30 min in PBST containing 5% normal goat serum. Sections were then incubated overnight with primary antibodies (polyclonal rabbit anti-ionized calcium binding adaptor molecule 1 [Iba1, which is specifically expressed in microglia and cells of monocytic lineage], 1:2000, Wako; polyclonal rabbit anti-glial fibrillary acidic protein [GFAP, which is specifically expressed in astrocytes], 1:10, Dako, Glostrup, Denmark; monoclonal mouse anti-microtubule-associated protein 2 [MAP-2, a neuron-specific marker], 1:400, Sigma) at 4 °C. Sections were washed three times with PBST and then incubated with a secondary antibody of an appropriate species (Alexa 594 goat anti-rabbit IgG (1:500) and Alexa 594 goat anti-mouse IgG (1:500), Invitrogen, Carlsbad, CA) at room temperature. Sections were then rinsed four times for 5 min in PBST, mounted onto slide glass (Matsunami, Osaka, Japan), and coverslipped with ProLong Gold antifade reagent (Invitrogen). Confocal fluorescent images were captured using a laser scanning confocal imaging system (Bio-Rad MRC-1024 on a Zeiss Axiophot inverted microscope) operated by Lasersharp 2000 software (Bio-Rad, Hercules, CA).

Assay of luciferase and protein determination. For the luciferase assay, different brain regions from mice, transplanted with luciferase-expressing bone marrow cells injected with LPS or saline were homogenized in 1 ml of ice-cold 50 mM Tris–HCl buffer (pH 7.0) containing complete protease inhibitor cocktail (Roche Diagnostics, Mannheim, Germany) using a Teflon homogenizer for 1 min on ice. The homogenates were centrifuged at 15,000 *g* for 15 min at 4 °C and the supernatants were used for a luciferase assay with PicaGene (Toyo, Tokyo, Japan) and the results are expressed in relative light units (RLU)/mg of protein. Protein concentrations were determined using a BCA protein assay kit (Pierce, Rockford, IL) with bovine serum albumin as the standard.

Statistics. Data were expressed as means ± SD for groups of 3 mice in FLI and 6 mice in BLI. Statistical analysis was performed using an analysis of variance (ANOVA) followed by Dunnett's test ($^{*}p < 0.05$ or $^{**}p < 0.01$ vs Day 0).

Results and discussion

Increased recruitment of bone marrow cells to the brain by intrahippocampal injection of LPS

Immunohistochemical experiments in rat have demonstrated that bone marrow cells infiltrate the brain after intrahippocampal injection of LPS [14]. In addition, it was observed that the number of activated microglia is significantly elevated from 1 to 28 days after intrahippocampal injection of LPS and reaches a maximum around day 7 [15]. Before we performed the *in vivo* imaging, we confirmed whether similar results could be obtained in chimeric mice that we generated by transplanting GFP-expressing bone marrow cells into irradiated wild-type mice. As the donor for GFP-expressing bone marrow cells, we chose enhanced GFP (EGFP) transgenic mice [12], because this mouse line possesses an EGFP

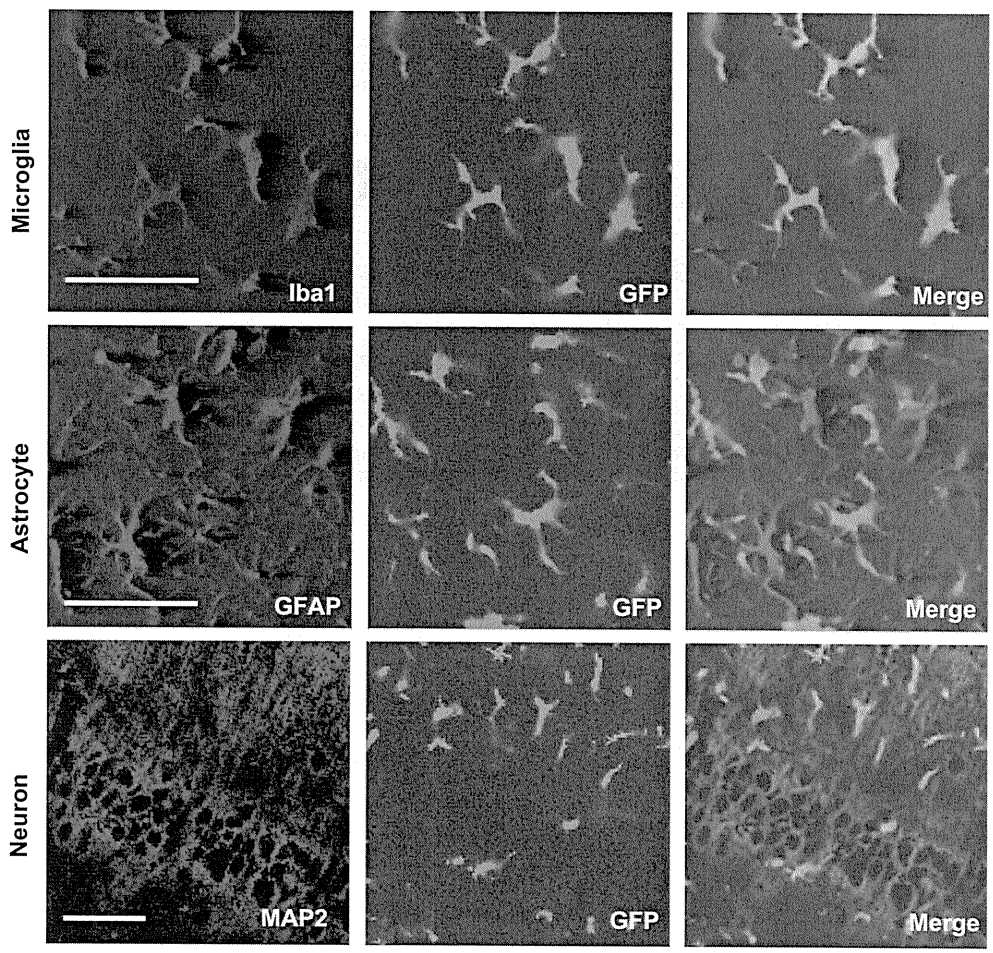

Fig. 2. Differentiation of bone marrow-derived cells into microglia. All panels show the presence of GFP-expressing bone marrow cells (green) in the hippocampus. Upper panels show examples of GFP positive/Iba1 positive (microglia in red) cells. Middle and lower panels are examples showing no expression of GFAP (astrocytes in red) and MAP2 (neurons in red) in bone marrow cells (green). Scale bars = 50 μm.

cDNA under the control of a chicken β-actin promoter and cytomegalovirus enhancer, so the GFP was constitutively expressed in cells.

Three months after the transplantation, we injected 1 μl of either saline or LPS (4 μg) directly into the hippocampus of these animals. The presence of GFP-positive cells in the brains was examined using coronal brain sections of animals sacrificed 7 days following LPS injection (Fig. 1). As expected, GFP-positive cells were observed in both LPS-injected brains and saline-injected control brains [16]. However, the number of GFP-positive cells in LPS-injected brains was significantly higher than that in controls (Fig. 1A and B). A weaker, but higher increase in GFP-positive cell penetration was also observed, even in areas distal to the injection site, such as the cortex and cerebellum (data not shown). The coexpression study showed that the expression of Iba1, which is a microglia maker, was observed in 100% of the GFP-positive cells, whereas MAP2 and GFAP, which are neuron and astrocyte markers, respectively, were not observed in the cells (Fig. 2), suggesting that the bone marrow-derived cells differentiated into microglia, but not into neurons or astrocytes. In addition, Iba1 positive cells in LPS-injected mice showed more inflammation-related activating morphology (ramified) than that of controls (Fig. 1B). These data indicated that bone marrow cells infiltrated to mouse brain and differentiated into microglia during brain inflammation because of the LPS injection.

In vivo fluorescence imaging of bone marrow-derived cells using GFP-expressing bone marrow chimeric mice

A marked increase in the penetration of GFP-positive cells into the brain was observed in coronal brain sections of the mice sacrificed on day 7 following intrahippocampal injection of LPS (Fig. 1). To visualize the dynamic changes of bone marrow cell infiltration with time, we performed FLI using chimeric mice over a 7-day period at multiple time points (postinjection days 0, 1, 3, 5, and 7). We injected LPS directly into the hippocampus of the animals and resected the skin of their scalps to prevent loss of signal by hair and skin (Fig. 3A). Saline-injected animals were used as controls. Fig. 3B shows representative data for FLI. A robust signal coming from the ROI was detected in both saline- and LPS-injected mice from day 1 with no significant differences. Contrary to our expectation, the signal intensity did not change over time and revealed no significant difference relative to saline controls by day 7 (Fig. 3C). The reason why we could not monitor the dramatic

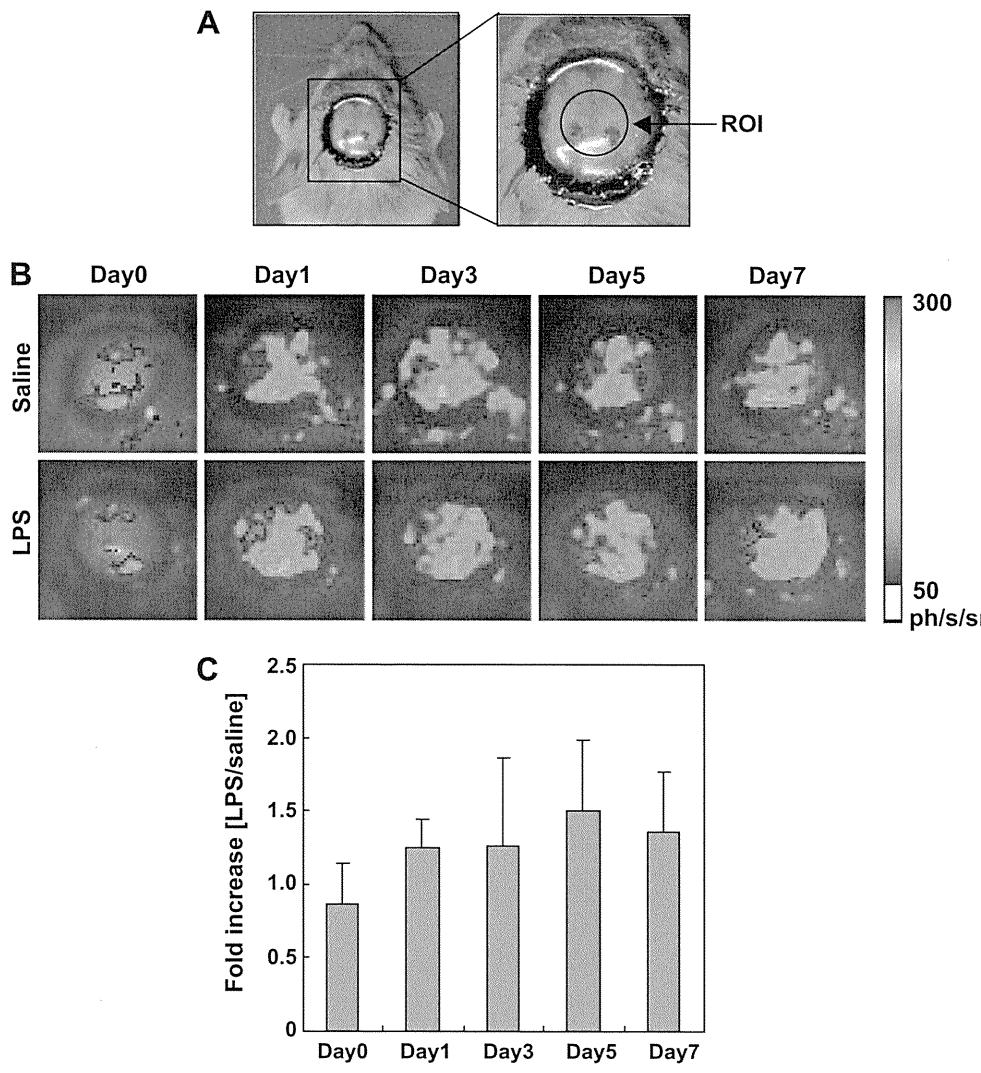

Fig. 3. *In vivo* fluorescence imaging of bone marrow-derived cells. (A) Cranial window. For better acquisition of the signal from the region of interest (ROI), the peripheral part of the cranial window was blackened with a felt-tip pen. (B) Representative *in vivo* fluorescence imaging of bone marrow-derived cells. (C) Quantitative analysis of bone marrow-derived cells related photon emissions. Robust signals were detected in both saline- and LPS-injected mice and observed no significant differences over time in saline vs LPS (means ± SD, $n = 3$).

changes of penetration of GFP-positive cells in brain inflammation is thought to be that the target GFP-positive cells were in a deep position (>2 mm, indicated by the arrow heads in Fig. 1A) and may not be excited at this depth by light from the apparatus used in this study. Furthermore, we only detected the signal from gatherings of GFP-positive cells on the surface of the brain, meninges, or cortex; the gathering of cells on surface of the brain was almost same between LPS- and saline-injected mice (Fig. 1A). FLI may therefore be unsuitable for monitoring the deep penetration of bone marrow cells into the brain.

In vivo bioluminescence imaging of bone marrow-derived cells using luciferase-expressing bone marrow chimeric mice

We next performed BLI using chimeric mice with luciferase-expressing bone marrow cells. BLI has been used recently to monitor and quantify gene activity in the same animal and to study disease progression in several organs [11]. Bioluminescence refers to light produced by the enzymatic reaction of a luciferase enzyme with its substrate. In this study, we used *mPer1-luc* transgenic mice with a firefly luciferase (FLuc) reporter on a C57BL/6J background as a donor of luciferase-expressing bone marrow cells [13] because it has been confirmed and accepted that the luciferase activity from identical tissue or cells from the mice show the same intensity at the same time of day. Thus, we performed BLI at the same time for every measurement in this study. In addition, it has been accepted that FLuc is a suitable luciferase for molecular imaging *in vivo* because its brightness increases at body temperature (37 °C) and the enzyme demonstrates a red shift (from 578 nm at 25 °C to 612 nm at 37 °C) [17]; hemoglobin is the primary chromophore that absorbs light within tissues [18], primarily in the blue and green part of the visible spectrum, but its absorption of wavelengths longer than 600 nm is reduced.

On the other hand, the substrate luciferin is thought to rapidly distribute throughout an animal after intraperitoneal (IP) injection and cross the BBB. The intensity of the photon emission changes with time, depending on the availability of the substrate at the monitoring site. Therefore, the dynamic profile of photon emission is of importance for the quantification of the signal. Thus, we first investigated its kinetic profile at the monitoring site after IP injection of D-luciferin using the chimeric mice. The profile shows a gradual increase followed by a slow decrease in photon emission and time-to-peak was found between 10 and 20 min (data not shown). So, we decided to perform the imaging at 15 min after IP injection of D-luciferin.

For BLI, we injected LPS directly into the hippocampus of the luciferase-expressing bone marrow chimeric mice and resected the skin of scalp as for FLI as shown in Fig. 3A. Saline-injected animals were used as controls. Fig. 4A shows representative data for longitudinal BLI. Longitudinal BLI demonstrated that the bioluminescence signal from the ROI increased from at least day 3 until the end of the study (Fig. 4B); Quantitation of the signals revealed a 15-fold increase (15.1 ± 5.9, $n = 6$) toward the saline injected controls at day 7. In order to determine whether the photons were being emitted from the hippocampus, brains were removed after the last BLI, rapidly dissected on a chilled platform to obtain different brain regions, and their luciferase activities measured *in vitro*. Higher activity was detected from all regions in LPS-injected animals and the highest and strongest activity was detected from the hippocampus (Fig. 4C). Quantitation of the signals from the hippocampus revealed a 14-fold increase (13.5 ± 5.9, $n = 5$) relative to the controls, which corresponds with that of BLI. These data indicate that BLI

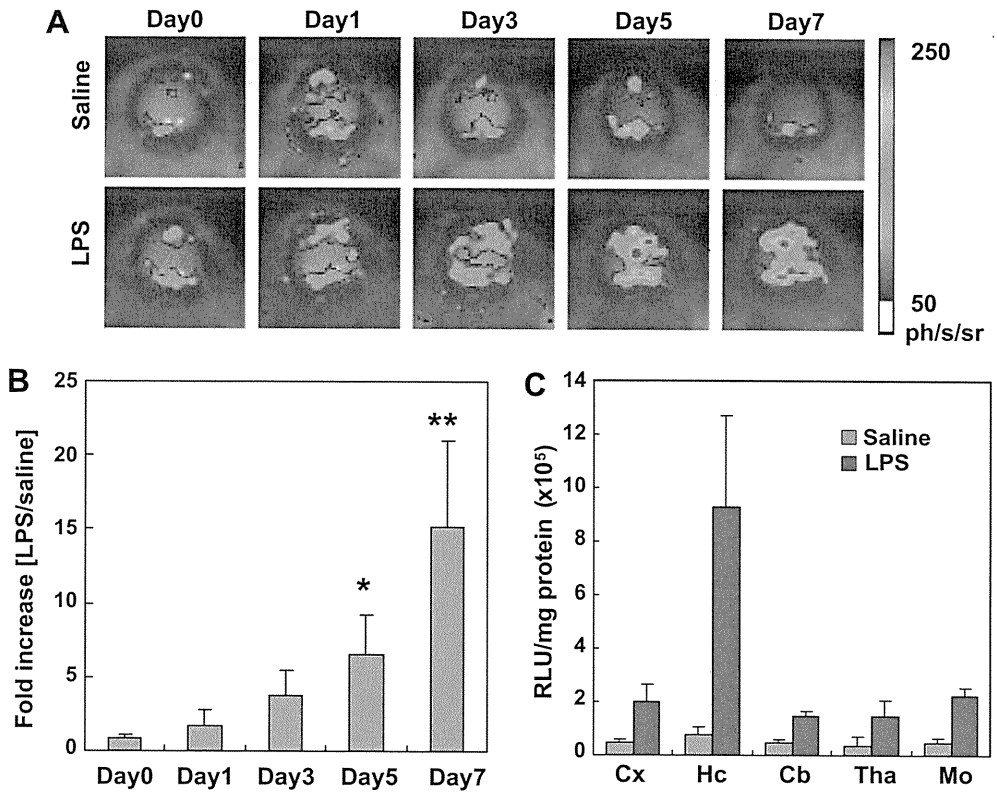

Fig. 4. *In vivo* bioluminescence imaging of bone marrow-derived cells. (A) Representative *in vivo* bioluminescence imaging of bone marrow-derived cells. (B) Quantitative analysis of bone marrow-derived cells related photon emissions. For statistical evaluation, ANOVA with Dunnett's test was applied, symbol · and ·· denote $P < 0.05$ and $P < 0.01$ vs Day 0, respectively, (mean ± SD, $n = 6$). (C) Luciferase activity in different brain regions of the luciferase-expressing bone marrow chimeric mice at day 7 after the last BLI (mean ± SD, $n = 5$). Cx, cortex; Hc, hippocampus; Cb, cerebellum; Tha, thalamus; Mo, medulla oblongata.

can monitor the penetration of bone marrow cells into the brain and is more suitable for such deep site monitoring than FLI.

Conclusion

In this study, we generated chimeric mice with GFP- or luciferase-expressing bone marrow cells, and performed FLI and BLI to monitor the infiltration of cells into brain during brain inflammation. Immunohistochemical investigation demonstrated that the infiltrated bone marrow cells differentiated into microglia. BLI, but not FLI, can successfully monitor increases in signal intensity that are derived from infiltration of luciferase-expressing bone marrow cells, indicating that BLI is more suitable for deep site monitoring in the brain than FLI. The chimeric mice with luciferase-expressing bone marrow could provide several new opportunities to study brain inflammation related injury, such as Parkinson's disease [7] and Alzheimer's disease [8,9], because of the observation of a markedly increased infiltration of bone marrow cells into the brain. The *in vivo* imaging tool described here may be useful for monitoring the protective effect of various drug treatments of brain inflammation, and contribute to the management of diseases with this condition.

Acknowledgments

The authors thank Kazuhiro Mino and Sanae Haga for their valuable instruction in the use of the *in vivo* imaging system. We also thank Sato Honma, Yoriko Ando, Toshiyuki Watanabe, and Kazutaka Yamada for their helpful advice and discussions. K.Y. and Y.O. was supported by grants from Takeda Science Foundation, Japan.

References

[1] N. Davoust, C. Vuaillant, G. Androdias, S. Nataf, From bone marrow to microglia: barriers and avenues, Trends Immunol. 29 (2008) 227–234.
[2] Y. Li, J. Chen, L. Wang, M. Lu, M. Chopp, Treatment of stroke in rat with intracarotid administration of marrow stromal cells, Neurology 56 (2001) 1666–1672.
[3] J. Priller, A. Flügel, T. Wehner, M. Boentert, C.A. Haas, M. Prinz, F. Fernández-Klett, K. Prass, I. Bechmann, B.A. de Boer, M. Frotscher, G.W. Kreutzberg, D.A. Persons, U. Dirnagl, Targeting gene-modified hematopoietic cells to the central nervous system: use of green fluorescent protein uncovers microglial engraftment, Nat. Med. 7 (2001) 1356–1361.
[4] D. Lu, Y. Li, L. Wang, J. Chen, A. Mahmood, M. Chopp, Intraarterial administration of marrow stromal cells in a rat model of traumatic brain injury, J. Neurotrauma 18 (2001) 813–819.
[5] A.R. Simard, S. Rivest, Neuroprotective effects of resident microglia following acute brain injury, J. Comp. Neurol. 504 (2007) 716–729.
[6] A. Flügel, M. Bradl, G.W. Kreutzberg, M.B. Graeber, Transformation of donor-derived bone marrow precursors into host microglia during autoimmune CNS inflammation and during the retrograde response to axotomy, J. Neurosci. Res. 66 (2001) 74–82.
[7] M. Rodriguez, L. Alvarez-Erviti, F.J. Blesa, M.C. Rodríguez-Oroz, A. Arina, I. Melero, L.I. Ramos, J.A. Obeso, Bone-marrow-derived cell differentiation into microglia: a study in a progressive mouse model of Parkinson's disease, Neurobiol. Dis. 28 (2007) 316–325.
[8] A.K. Stalder, F. Ermini, L. Bondolfi, W. Krenger, G.J. Burbach, T. Deller, J. Coomaraswamy, M. Staufenbiel, R. Landmann, M. Jucker, Invasion of hematopoietic cells into the brain of amyloid precursor protein transgenic mice, J. Neurosci. 25 (2005) 11125–11132.
[9] A.R. Simard, D. Soulet, G. Gowing, J.P. Julien, S. Rivest, Bone marrow-derived microglia play a critical role in restricting senile plaque formation in Alzheimer's disease, Neuron 16 (2006) 489–502.
[10] J. Lippincott-Schwartz, G.H. Patterson, Development and use of fluorescent protein markers in living cells, Science 300 (2003) 87–91.
[11] C.H. Contag, M.H. Bachmann, Advances in *in vivo* bioluminescence imaging of gene expression, Annu. Rev. Biomed. Eng. 4 (2002) 235–260.
[12] M. Okabe, M. Ikawa, K. Kominami, T. Nakanishi, Y. Nishimune, 'Green mice' as a source of ubiquitous green cells, FEBS Lett. 407 (1997) 313–319.
[13] N. Inagaki, S. Honma, D. Ono, Y. Tanahashi, K. Honma, Separate oscillating cell groups in mouse suprachiasmatic nucleus couple photoperiodically to the onset and end of daily activity, Proc. Natl. Acad. Sci. USA 104 (2007) 7664–7669.
[14] K.A. Ji, M.Y. Eu, S.H. Kang, B.J. Gwag, I. Jou, E.H. Joe, Differential neutrophil infiltration contributes to regional differences in brain inflammation in the substantia nigra pars compacta and cortex, GLIA 56 (2008) 1039–1047.
[15] D.L. Herber, J.L. Maloney, L.M. Roth, M.J. Freeman, D. Morgan, M.N. Gordon, Diverse microglial responses after intrahippocampal administration of lipopolysaccharide, GLIA 53 (2006) 382–391.
[16] A.R. Simard, S. Rivest, Bone marrow stem cells have the ability to populate the entire central nervous system into fully differentiated parenchymal microglia, FASEB J. 18 (2004) 998–1000.
[17] H. Zhao, T.C. Doyle, O. Coquoz, F. Kalish, B.W. Rice, C.H. Contag, Emission spectra of bioluminescent reporters and interaction with mammalian tissue determine the sensitivity of detection *in vivo*, J. Biomed. Opt. 10 (2005) 41210.
[18] V. Tuchin, Tissure Optics, SPIE Press, Bellingham, WA, 2000.

Journal of Surgical Research **152,** 218–223 (2009)
doi:10.1016/j.jss.2008.02.059

Autonomic Regulation of Liver Regeneration After Partial Hepatectomy in Mice

Osamu Ikeda, M.D.,* Michitaka Ozaki, M.D., Ph.D.,† Soichiro Murata, M.D., Ph.D.,* Ryota Matsuo, M.D., Ph.D.,* Yoritaka Nakano, M.D.,* Motonobu Watanabe, M.D.,* Katsuji Hisakura, M.D.,* Andriy Myronovych, M.D.,* Takuya Kawasaki, M.D.,* Keisuke Kohno, M.D.,* and Nobuhiro Ohkohchi, M.D., Ph.D.*,[1]

**Department of Surgery, Advanced Biomedical Applications, Graduate School of Comprehensive Human Sciences, University of Tsukuba, Tsukuba, Japan; and †Department of Molecular Surgery, Hokkaido University School of Medicine, Sapporo, Japan*

Submitted for publication November 15, 2007

Background/Aims. **The autonomic vagus nerve is thought to play an essential role in liver regeneration since hepatic vagotomy delays hepatic DNA synthesis. However, how the parasympathetic vagus nerve is involved in liver regeneration remains obscure. Kupffer cells are located in liver sinusoids adjacent to hepatocytes and might regulate liver regeneration by releasing interleukin-6 (IL-6). The present study examines the role of the vagus nerve and how Kupffer cells are involved in parasympathetic nerve-mediated liver regeneration in mice.**

Methods. **We performed surgical vagotomy of the hepatic branch and then partial hepatectomy (PH); some mice received acetylcholine (ACh) agonist/antagonist before PH. We then evaluated liver regeneration and signal transducer and activator of transcription-3 (STAT3) activation. We also investigated whether ACh stimulates IL-6 release from Kupffer cells.**

Results. **Surgical vagotomy impaired liver regeneration. STAT3, which is activated by IL-6 after hepatectomy and plays a pivotal role in liver regeneration, was less activated in vagotomized mice after PH. Post-PH STAT3 activation was recovered by administering vagotomized mice with an ACh agonist. Furthermore, ACh stimulated IL-6 release in Kupffer cells *in vitro*.**

Conclusion. **The parasympathetic system (vagus nerve) contributes to liver regeneration after hepatectomy by stimulating IL-6 release from Kupffer cells followed by STAT3 activation in hepatocytes.**

Key Words: **liver regeneration; vagus nerve; Kupffer cells; IL-6; STAT3; acetylcholine.**

INTRODUCTION

The liver regenerates through the proliferation of all extant mature cellular populations and is not dependent on progenitor or stem cells [1, 2]. Liver regeneration is a critical issue related to clinical morbidity and mortality in drug-induced liver injury, and after surgery including hepatectomy or transplantation [3–5]. Various genes that are related to hepatic growth and proliferation are expressed within hours after partial hepatectomy (PH) [6] and DNA is synthesized in hepatocytes 12 to 16 h and peaks 40 to 44 h after PH in mice [7–9]. The structural and functional regeneration of the liver requires strictly and chronologically regulated processes of initiation, maintenance, and termination of liver growth.

The initiation of liver regeneration requires appropriate mitogenic stimulation of hepatocytes [1]. Interleukin-6 (IL-6) is considered a key cytokine in liver regeneration and is the principal activator of signal transducer and activator of transcription-3 (STAT3) [10–12]. STAT3 plays a critical role in cell proliferation and is activated during the early phase of liver regeneration after PH [13]. Kupffer cells are resident macrophages in the liver and comprise the primary source of IL-6 produced in the liver [14]. Therefore, they might play a key role in liver regeneration.

[1] To whom correspondence and reprint requests should be addressed at Department of Surgery, Advanced Biomedical Applications, Graduate School of Comprehensive Human Sciences, University of Tsukuba, 1-1-1 Tennodai, Tsukuba, Ibaraki 305-8575, Japan. E-mail: nokochi3@md.tsukuba.ac.jp.

0022-4804/09 $36.00

The autonomic nervous system influences many fundamental functions of various organs, including those of the cardiovascular, digestive, urogenital, and endocrine systems. The liver is also directly innervated and regulated by autonomic nerves [15]. The vagus nerve is considered to play an essential role in liver regeneration since hepatic vagotomy delays the increase in the rate of hepatic DNA synthesis [16–18]. One of the neuropeptides, thyrotropin-releasing hormone, acts in the central nerve system to stimulate hepatic DNA synthesis and the stimulatory effect is blocked by hepatic branch vagotomy [19]. The sympathetic nerve was proven to have no influence on liver regeneration [17], but Oven *et al.* reported that sympathectomy increases hepatic progenitors and reduces liver injury [20]. Total liver denervation promotes liver regeneration in rats [21]. Nevertheless, the precise mechanism of the autonomic nerve system in the regulation of liver regeneration remains obscure.

The vagus nerve and macrophages are closely associated. During inflammation, the vagus nerve mainly suppresses acute inflammatory reactions by inhibiting the release of pro-inflammatory cytokines such as tumor necrosis factor-alpha (TNF-α) and IL-6 [20–22]. One mechanism is associated with the vagus nerve in which acetylcholine (ACh) or ACh agonist inhibits cytokine release from resident tissue macrophages [22–26]. Therefore, the vagus nerve might affect liver regeneration by regulating cytokine release from Kupffer cells. However, the effect of the vagus nerve on Kupffer cells during liver regeneration is not understood in detail.

Here, we examined the role and mechanism of the vagus nerve on liver regeneration in a conventional mouse model of PH.

MATERIALS AND METHODS

Animals

Eight-week-old male C57BL/6 mice (Charles River Japan, Yokohama, Japan) weighing 20 to 25 g were maintained in a temperature-controlled room on a 12-h light-dark cycle with free access to water and standard chow. All animal experiments proceeded in a humane manner after receiving approval from the Institutional Animal Experiment Committee of the University of Tsukuba, and in accordance with the Regulation for Animal Experiments at our university and the Fundamental Guideline for Proper Conduct of Animal Experimentation and Related Activities in Academic Research Institutions under the jurisdiction of the Ministry of Education, Culture, Sports, Science and Technology of Japan.

Experimental Design

Experiment 1 examined the effect of hepatic vagotomy on liver regeneration and experiment 2 examined the effect of the vagus nerve on cytokine release by measuring the effect of ACh on cytokine production from Kupffer cells *in vitro*.

Experiment 1

Mice were divided into a group that underwent hepatic branch vagotomy and a control group that underwent a sham operation. All mice underwent 70% PH 1 wk after vagotomy or sham operation. Five to 10 mice from each group were sacrificed and liver specimens were collected at 2, 24, 48, and 72 h after PH. In an additional experiment, 5 vagotomized mice received an intraperitoneal injection of the selective nicotinic AChR agonist, anabasine (Sigma Chemical Co., St. Louis, MO) (4 mg/kg) and 5 control mice received the nonselective nicotinic AChR antagonist, mecamylamine (Sigma Chemical Co.) (1 mg/kg), 15 min before PH and were sacrificed 2 h after PH.

Experiment 2

Murine Kupffer cells cultured for 24 h in RPMI 1640 medium containing 10% fetal calf serum were further incubated with or without 100 μM of ACh. The control group was incubated with the same volume of saline added to the medium.

Surgical Procedures

Surgery proceeded under ether anesthesia. Hepatic branch vagotomy was achieved by selectively sectioning the hepatic branch of the vagus nerve that branches off from the left main vagal trunk [17]. The hepatic branch of the vagus nerve was exposed without resection in the control group. These operations were performed 1wk before PH to exclude the effects of their surgical stresses. PH was performed as described by Higgins and Anderson [27]. Briefly, the left and median lobes of the liver were removed with a single ligature under ether anesthesia. The mice were then returned to their cages and given free access to food and water.

Cell Proliferation Assay

We counted mitotic hepatocytes and proliferating cell nuclear antigen (PCNA)-positive hepatocytes to assess cell proliferation of hepatocytes after PH. Liver tissues were removed at 24 and 48 h after PH, fixed in 10% buffered formalin, embedded in paraffin and stained with hematoxylin and eosin (H and E) and with anti-PCNA using a kit (Zymed Laboratories Inc., San Francisco, CA). The ratio (%) of mitotic or PCNA-positive hepatocytes was calculated at least three times in different sections from each group at 200-fold magnification.

Western Blotting

Liver protein extracts were separated by 10% sodium dodecyl sulfate-polyacrylamide gel electrophoresis, transferred to nitrocellulose membranes (Millipore, Bedford, MA) and blotted against the primary antibodies, STAT3/phospho-STAT3 (Tyr705), Akt/phospho-Akt (Ser473) (Cell Signaling, Beverly, MA), followed by secondary goat and mouse antibodies conjugated with horseradish peroxidase (Zymed Laboratories Inc). The relative density of protein bands was determined using Scan Analysis image quantitation software (Scion Image Beta 4.0.3, Frederick, MD).

Isolation and Culture of Kupffer Cells

Kupffer cells were isolated from mice as described with some modification [28]. Briefly, the liver was perfused through the portal vein with Ca^{2+}- and Mg^{2+}-free Hank's balanced salt solution at 37°C for 3 min at a flow rate of 10 mL/min, followed by Hank's balanced salt solution containing 0.05% Type 1 collagenase (Sigma Chemical Co.) at 37°C for 8 min. Thereafter, the liver was excised and cut into small pieces in buffer containing collagenase. The suspension was filtered through nylon gauze and the filtrate was centrifuged twice at 50 × g for 3 min at 4°C to pellet parenchymal cells. The remaining

cell fraction in the supernatant was resuspended in complete William's E medium containing 10% heat-inactivated fetal calf serum and allowed to adhere to the bottom of plastic culture dishes for 15 min. Free cells were removed by gentle washing. The purity of the adherent Kupffer cells was immunohistologically assessed using the rat anti-mouse macrophage monoclonal antibody F4/80 (Serotec, Raleigh, NC) (data not shown).

Enzyme-Linked Immunosorbent Assay for IL-6

The concentration of IL-6 in the medium of Kupffer cell cultures was determined using a mouse specific IL-6 enzyme-linked immunosorbent assay kit (R and D Systems, Minneapolis, MN).

Reverse Transcriptase Polymerase Chain Reaction for IL-6

Total cellular RNA was isolated from cultured Kupffer cells using Isogen reagent (Nippon Gene, Tokyo, Japan). First-strand cDNA was synthesized using reverse transcriptase, 2 μg of total RNA, and oligo (dT) primers. The cDNA was amplified by PCR with IL-6 and mouse β-actin. The primers for IL-6 and β-actin were 5′-CTGGTGACAACCACGGCCTTCCCTA-3′ and 5′-ATGCTTAGGACTAACGCACTAGGT-3′, 5′-CCCAGAGCAAGAGAGGTATC-3′ and 5′-AGAGCATAGCCCTCGTAGAT-3′, respectively. The PCR products were separated on 2% agarose gels.

Statistical Analysis

Results are expressed as means ± S.D. Data were analyzed using the Mann-Whitney *t*-test, and *P*-values below 0.05 were considered statistically significant.

RESULTS

Experiment 1—Liver Mass Recovery After PH in Surgically Vagotomized Mice

The liver/body weight ratio 48 h after PH in the vagotomy group was significantly lower than that in the control group. At 2, 24, and 72 h after PH, there was no significant difference between the groups, although the liver tended to recover slowly in the vagotomy group (Fig. 1).

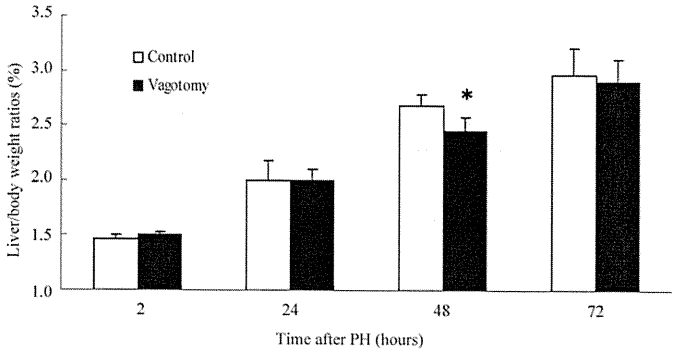

FIG. 1. Changes in liver/body weight ratio after PH in control and vagotomized mice. Five to 10 mice were sacrificed at 2, 24, 48, and 72 h after PH. Data are presented as means ± S.D. $^*P < 0.05$ versus control group.

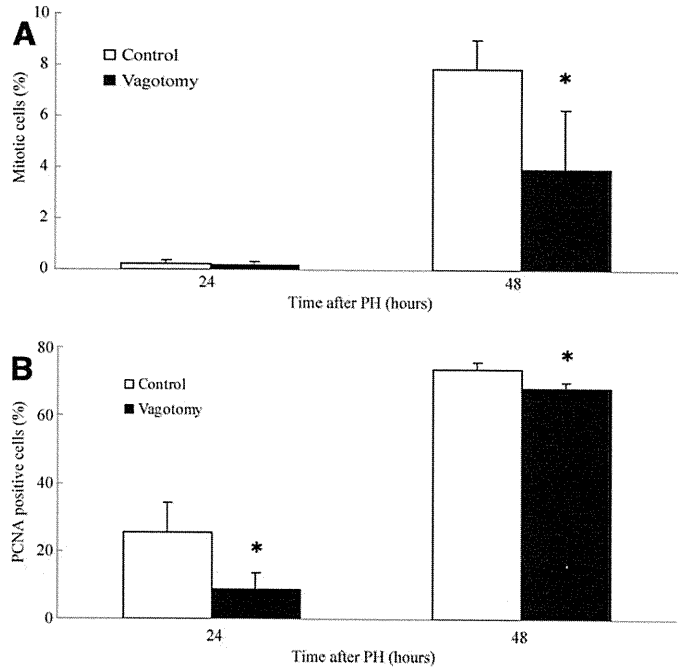

FIG. 2. Hepatocyte proliferation after PH. (A) Mitotic hepatocytes 24 and 48 h after PH counted in triplicate on different sections. (B) PCNA positive hepatocytes 24 and 48 h after PH counted in triplicate on different sections. Data are presented as means ± S.D ($n = 6$ per group). $^*P < 0.05$ *versus* control group.

Hepatocyte Proliferation After PH in Vagotomized Mice

Histological examination of residual liver revealed numerous mitotic hepatocytes in the regenerating liver in the control group at 48 h after PH, but fewer in the vagotomy group (Fig. 2A). Immunohistochemical staining of PCNA also confirmed that the mitotic activity of hepatocytes reduced and delayed in the vagotomy group (Fig. 2B).

Activation of STAT3 and Akt in the Vagotomy Group

We examined STAT3 and Akt activation to understand the effect of vagotomy on cellular signaling pathways. Both STAT3 and Akt were phosphorylated immediately after PH in the control group, whereas STAT3 phosphorylation was partially but significantly suppressed in the vagotomy group although its protein levels did not change (Fig. 3A). The phosphorylation of Akt did not significantly differ between the groups (Fig. 3B).

Effect of AChR Agonist and Antagonist on Activation of STAT3

We examined whether pharmacological stimulation of AChR influences STAT3 activity. Vagotomized and sham-operated control mice underwent PH 15 min after the administration of anabasine (AChR agonist) and mecamylamine (AChR antagonist), respectively. Post-PH STAT3 phosphorylation was obviously sup-